

DOT/FAA/AR-00/74

Office of Aviation Research
Washington, D.C. 20591

Assessment of Probabilistic Certification Methodology for Composite Structures

January 2001

Final Report

This document is available to the U.S. public
through the National Technical Information
Service (NTIS), Springfield, Virginia 22161.



U.S. Department of Transportation
Federal Aviation Administration

NOTICE

This document is disseminated under the sponsorship of the U.S. Department of Transportation in the interest of information exchange. The United States Government assumes no liability for the contents or use thereof. The United States Government does not endorse products or manufacturers. Trade or manufacturer's names appear herein solely because they are considered essential to the objective of this report. This document does not constitute FAA certification policy. Consult your local FAA aircraft certification office as to its use.

This report is available at the Federal Aviation Administration William J. Hughes Technical Center's Full-Text Technical Reports page: actlibrary.tc.faa.gov in Adobe Acrobat portable document format (PDF).

1. Report No. DOT/FAA/AR-00/74		2. Government Accession No.		3. Recipient's Catalog No.	
4. Title and Subtitle ASSESSMENT OF PROBABILISTIC CERTIFICATION METHODOLOGY FOR COMPOSITE STRUCTURES				5. Report Date January, 2001	
				6. Performing Organization Code	
7. Author(s) Han-Pin Kan				8. Performing Organization Report No.	
9. Performing Organization Name and Address Northrop Grumman Corporation Integrated Systems and Aerostructures One Hornet Way El Segundo, CA 90245-2804				10. Work Unit No. (TRAIS)	
				11. Contract or Grant No. DTFA03-98-F-IA024, 437-25-24	
12. Sponsoring Agency Name and Address U.S. Department of Transportation Federal Aviation Administration William J. Hughes Technical Center				13. Type of Report and Period Covered Final Report	
				14. Sponsoring Agency Code AIR-120	
15. Supplementary Notes FAA William J. Hughes Technical Center Technical Monitor: Peter Shyprykevich					
16. Abstract A sensitivity study has been conducted to assess the currently available probabilistic structural analysis methods. The influence of the distribution parameters on the probability of failure was investigated analytically. The significant parameters that have an impact on development of probabilistic certification procedures were identified. The technical gaps which need to be filled for probabilistic certification of composite structures were discussed.					
17. Key Words Probability, Monte Carlo simulation, Load distribution, Operational damage, Manufacturing defect, Certification,			18. Distribution Statement Document is available to the public through the National Technical Information Service, Springfield, Virginia 22161		
19. Security Classif.(of this report) Unclassified	20. Security Classif.(of this page) Unclassified	21. No. of Pages 58	22. Price		

TABLE OF CONTENTS

	Page
EXECUTIVE SUMMARY	vii
1. INTRODUCTION	1
2. ASSESSMENT OF CURRENT PROBABILISTIC DESIGN METHODS	1
2.1 The NGCAD Methodology	2
2.2 The TsAGI Methodology	3
2.3 Northrop Grumman Commercial Aircraft Division and TsAGI Probabalistic Methodologies	5
2.4 Example Application of the NGCAD and TsAGI's Methods	6
2.4.1 Structural Model	6
2.4.2 Load Truncation and Design Factor	8
2.4.3 Baseline Thickness	8
2.4.4 Surface Area	9
2.4.5 Number of $\pm 45^\circ$ Plies	9
2.4.6 Failure Modes	9
2.4.7 Margin of Safety at Critical Locations	10
2.4.8 Allowables	11
2.4.9 Statistical Distribution of Stresses	12
2.4.10 Manufacturing Defects	13
2.4.11 Moisture and Temperature Degradation Effects	14
2.4.12 Operational Defects	14
2.4.13 Skin Temperature Distribution	15
2.4.14 Probability of Damage Detection	15
2.4.15 Repair	16
2.4.16 Comparison of Results	16
3. SENSITIVITY STUDIES USING THE NGCAD METHODOLOGY	17
3.1 Convergence of Results	17
3.2 Sensitivity of Load Distribution Function	24
3.3 Sensitivity of Operational Damage Parameters	29
3.4 Sensitivity of Manufacturing Defect Parameters	36
3.5 Equivalent Factor of Safety	40
3.6 Transport Wing Structure	42
4. PROBABILISTIC CERTIFICATION METHODOLOGY	47

4.1	Analysis	48
4.2	Testing	49
5.	CONCLUSIONS	49
6.	REFERENCES	50

LIST OF FIGURES

Figure		Page
1	Empirical Exceedance of Damage Rate, All Data	5
2	Northrop Grumman Commercial Aircraft Division Model of Lear Fan 2100 Wing	7
3	Central Aerohydrodynamic Institute Model of Lear Fan 2100 Wing	8
4	Extrapolated Exceedance Curve for the Lear Fan Analysis	13
5	Averaged Overall Failure Probability Versus Number of Monte Carlo Simulations	18
6	Average Probability of Failure at the Most Critical Location	19
7	Average Probability of Failure for Group 2 Panels	20
8	Average Probability of Failure for Group 3 Panels	20
9	Average Probability of Failure for Group 4 Panels	21
10	Average Probability of Failure for the Overall Lear Fan Model, Based on 1000 Simulations in Each Set	23
11	Average Probability of Failure for the Overall Lear Fan Model, Based on 5000 Simulations in Each Set	23
12	Average Probability of Failure for the Overall Lear Fan Model, Combined Results	24
13	Baseline PDFs for the Lear Fan Wing Skins and Substructures	25
14	Wing Skin Load Factor PDF With Variable Log Means	25
15	Effects of Load Factor Distribution Mean on the Overall Probability of Failure	26
16	Wing Skin Load Factor PDF With Variable σ	27
17	Effects of Load Factor Distribution σ on the Overall Probability of Failure	27

18	Skin Load Factor Distributions With Variable Shift Factor in the Lognormal Distribution	28
19	Effects of Load Distribution Shift Factor on the Failure Probability	28
20	Overall P_f for $R_o = 1.00e^{-08}$	30
21	Overall P_f for $R_o = 2.00e^{-08}$	30
22	Overall P_f for $R_o = 5.00e^{-08}$	31
23	Overall P_f for $R_o = 1.00e^{-07}$	31
24	Overall P_f for $R_o = 1.00e^{-06}$	32
25	Sensitivity of the Overall Failure Probability to Upper Skin MID Rate	32
26	Effects of Operational Damage Parameter Fc_o on P_f	33
27	Relative P_f for Location 1 With Variable R_o for MID	34
28	Relative P_f for Location 4 With Variable R_o for MID	34
29	Relative P_f for Location 28 With Variable R_o for MID	35
30	Relative P_f for Location 1 With Variable Fc_o for MID	35
31	Relative P_f for Location 4 With Variable Fc_o for MID	36
32	Relative P_f for Location 28 With Variable Fc_o for MID	36
33	Influence of the Manufacturing Defect Parameters on P_f , $R_m = 0.005$	38
34	Influence of the Manufacturing Defect Parameters on P_f , $R_m = 0.0005$	38
35	Influence of the Manufacturing Defect Parameters on P_f , $R_m = 0.00005$	38
36	Relative P_f Sensitivity of Manufacturing Defect Parameters at Location 1	39
37	Relative P_f Sensitivity of Manufacturing Defect Parameters at Location 28	39
38	Relative P_f Sensitivity of Manufacturing Defect Parameters at Location 44	40
39	Probability of Failure Versus Equivalent Factor of Safety	41
40	Probability of Failure Versus Equivalent Factor of Safety for the Compression Critical Locations	41
41	Probability of Failure Versus Equivalent Factor of Safety for the Tension Critical Locations	42

LIST OF TABLES

Table		Page
1	Empirical Constants for Damage Rate	5
2	Comparison of the Surface Areas in the Two Models	9
3	Comparison of Margin of Safety in the Two Models	11
4	Cumulative Probability of Damage Occurrence	14
5	Flight Lifetime Temperature Distribution of the Lear Fan 2100 Aircraft	15
6	Probability of Damage Detection in the TsAGI Analysis	16
7	Comparison of Results	16
8	Number of Monte Carlo Simulations for Approximate Probability of Failure	22
9	Parameters for the Load Factor Distribution	24
10	Effects of MID Damage Rate on Failure Probability	29
11	Effects of Compressive Strength Reduction Factor From Operational Damage On P_f	33
12	Summary of the Manufacturing Defect Parameter Sensitivity	37
13	Locations for the Boeing C-X Wing Upper Skin	43
14	Overall Temperature Distribution of the C-X Transport Upper Wing Skin	43
15	Estimated Moisture History for the Upper Wing Skin	44
16	Compression Strength Reduction Due to Manufacturing Defects	45
17	Effects of Load Distribution Parameter on the C-X Upper Wing Skin P_f	46
18	Sensitivity of the Upper Wing Skin Failure Probability to FC_o	46
19	Sensitivity of the Wing Upper Skin Failure Probability to Design Allowable Strain	47

EXECUTIVE SUMMARY

The application of composite materials to primary aircraft structures requires proven certification procedures for demonstration of structural integrity. In the development of certification procedures, the inherent characteristics of composites must be recognized. One of these characteristics is the variability in strength and fatigue life data. The variability, although higher than that observed in metals, does not negate the weight efficiency of composites structures and must be accounted for in the certification process. Because of the strength and fatigue data scatter in composites, the structural reliability provided by the conventional deterministic certification approach (using the same factor of safety) is different for composite and metal structures. In order to certify composite structures with the same level of confidence as metallic structures, a probabilistic-based methodology is of interest. In addition to the scatter in strength and life data, the uncertainties of the applied loads also affect the reliability of a structure. A factor of safety of 1.5, traditionally used in aircraft structural design, generally provides a very high level of reliability. However, this approach is not capable of quantifying the reliability of a composite structural design. The probabilistic certification method will provide additional information which can be used for a more efficient structural design.

The objective of this program was to assess the suitability of the probabilistic approach for the certification of composite structures and to identify the elements needed for the development of such a methodology. A technology assessment was conducted on the current probabilistic certification methodology. A sensitivity study, using existing probabilistic methods and available composite aircraft structures, was carried out to identify key parameters.

As a result of this program, the analytical and experimental need to establish a probabilistic structural certification procedure has been identified. Certification criterion has been proposed and the state-of-the-art capability of the probability structural analysis was assessed.

1. INTRODUCTION.

The application of composite materials to primary aircraft structures requires proven certification procedures for demonstration of structural integrity. In the development of certification procedures, the inherent characteristics of composites must be recognized. One of these characteristics is the variability in strength and fatigue life data. This variability, while higher than that observed in metals, although not negating the weight efficiency of composite structures, must be accounted for in the certification process. Because of the strength and fatigue data scatter in composites, the structural reliability provided by the conventional deterministic certification approach is different for composite and metal structures. In order to certify composite structures with the same level of confidence as metallic structures, a probabilistic-based methodology is of interest. In addition to the scatter in strength and life data, the uncertainties of the applied loads also affect the reliability of a structure. A factor of safety of 1.5, traditionally used in aircraft structural design, generally provides a very high level of reliability. However, a safety of factor approach cannot be used to assess the risk involved in a structural design. The probabilistic certification method will provide this additional information which can be used for more efficient structural design.

The Federal Aviation Administration (FAA) has published Advisory Circular (AC) 20⁻¹⁰7A [1] as a certification guide for composite structures. An overview of FAA composite certification activities is presented in reference 2, while the important considerations of AC 20⁻¹⁰7A can be found in reference 3. The FAA has also funded a series of research programs [4-9] to evaluate various approaches to static strength and fatigue life certification of composite structures. A probabilistic design methodology developed recently under Interagency Agreement DTFA03-84-A-40021 by Northrop Grumman Commercial Aircraft Division (NGCAD) is discussed in reference 10. A continuation of that work is reported in reference 11. A brief assessment of the FAA certification activities described in references 2 through 9 indicates that a comprehensive probabilistic methodology may be advantageous.

The objective of this program was to assess the suitability of the probabilistic approach for the certification of composite structures and to identify the critical elements encountered in the development of such a methodology. This was done using two methodologies [10 and 12] and one software program [10] developed under FAA funding. A sensitivity study, using these probabilistic methods and available composite aircraft structures, was carried out to identify key parameters. Finally, based on the results of the sensitivity study, a certification approach is suggested for FAA consideration.

2. ASSESSMENT OF CURRENT PROBABILISTIC DESIGN METHODS.

A review of probabilistic design methodology for composite structures was conducted by NGCAD and the results were documented in references 10 and 11. The technology assessment effort in the present study focused on comparing the method in reference 10, the NGCAD method, and the method in reference 12, the Central Aerohydrodynamic Institute (TsAGI) method. A brief discussion of the two methods is first presented and a detailed comparison of the methods applied to a composite structure is then given.

2.1 THE NGCAD METHODOLOGY.

The NGCAD probabilistic design methodology employs a numerical integration scheme with Monte Carlo simulation to determine probability of failure of a structural component or system of structural components.

The basic equation used to calculate the probability of failure for each Monte Carlo simulation accounting for the random effect of gust, environment, and defects is given by:

$$P_f = \int_{\Omega_s} f(s)G(s)ds \quad (1)$$

Where: $f(s)$ is the probability density function (PDF) of the adjusted σ_{max} per flight for a randomly selected gust magnitude

$G(s)$ is the cumulative density function (CDF) of the adjusted material strength for a set of randomly selected values accounting for effects of environments and defects,

Ω_s is the domain of s .

A numerical integration method is used. The overall probability of failure of a structural component or system is obtained by finding the average value of P_f in equation 1 from all simulations. The PDF of the unadjusted maximum operational stress (σ_{max}) per flight is determined from the maximum vertical load factor ($n_{z,max}$) per flight PDF and the relationship between n_z and σ . The program accommodates normal, lognormal, and Weibull PDF types. The baseline material strength is also expressed in terms of an appropriate PDF.

The margin of safety at each structural location is determined from a deterministic analysis and used to define the design limit stress at the selected location. Knowing the n_z level corresponding to design limit load, a scale factor is used to convert the maximum n_z per flight PDF into stress units consistent with those of the material strength PDF.

The NGCAD method includes the effects of manufacturing defects and operational damage on the reliability of the structure. The manufacturing defects are accounted for by applying a knockdown factor to the material strength. This factor is defined by the nature, severity, and frequency of occurrence of the defects. The effects of operational damage are also accounted for by a factor that is defined by the source, effects, and frequency of damage. A single material strength scale factor is used to adjust the strength distribution.

The major steps in each Monte Carlo simulation are (1) randomly adjust the stress and strength PDFs to account for the stochastic effects of environment, gust loading, and other influences, and (2) calculate P_f for each simulation using equation 1 for a set of randomly selected values by a numerical integration method. At the end of the simulations, the average P_f from all simulations is calculated. An analysis software titled "MONTE" was developed by NGCAD for probabilistic evaluation of composite structures.

Other parameters required in the NGCAD method are:

- Usage requirements
- Load parameters
- Structural design parameters
- Material strength parameters
- Operating environment

The NGCAD method utilizes stress analysis results from conventional design methods. Finite element analysis (FEA) is not part of the NGCAD probabilistic analysis, but the results of FEA provide input to the probability analysis. Deterministic values of thickness and margin of safety together with the critical failure mode predicted by the FEA are used as baseline parameters to select low margin of safety locations for probabilistic analysis.

A linear scale factor is used to convert load factor to stress or strain. The scale factor is obtained from the input design allowable and the margin of safety (M.S.) as shown in the following equation.

$$\text{Scale factor} = \text{design allowable} / (1.5 \cdot (1 + \text{M.S.})) / \text{load factor at limit load}$$

In each Monte Carlo simulation, a random load factor is drawn from the load distribution function. The load factor is then multiplied by the scale factor to obtain the strain. For example, if the margin of safety of a structural element is 0.68, the allowable strain is 5000 μ -in/in in compression, and the load factor at limit load is 3.29g, then the strain at design ultimate load (DUL) is ϵ with $5000/\epsilon - 1 = 0.68$, $\epsilon = 2976 \mu$ -in/in, and the strain at design limit load (DLL) is $2976/1.5 = 1984 \mu$ -in/in. Finally, the scale factor is $1984/3.29 = 603.08$. This scale factor is then used as the linear conversion factor. Assuming a load factor of 2.89 g to result from a random draw from the load distribution, the corresponding strain is then $2.89 \cdot 603.08 = 1743 \mu$ -in/in.

2.2 THE TsAGI METHODOLOGY.

As described in reference 12, the analysis software titled “**Probabilistic Design of Damage Tolerant Composite Aircraft Structures (ProDECompos)**” developed by Ushakov, et al. provides designers, engineers, and analysts with an automated means for:

- Damage tolerance and reliability analysis of composite aircraft structures with manufacturing defects and in service damage.
- Formulating and substantiating the set of measures to be undertaken during design, manufacturing, certification, and service for specified level of safety and reliability (i.e., establish safety and reliability goals for design, manufacturing, certification, and service of composite structures.)

The probabilistic analysis used in the TsAGI methodology uses Monte Carlo simulation. In the TsAGI approach the distributions of stress and material strength are subjected to lifetime properties of material quality, manufacturing quality, operational structural damage (including maintenance induced damage, etc.), and operating environment (temperature, moisture, and sun

radiation). The final stress and strength distributions are established by accounting for the impact of all these random risk drivers. The probability of failure is then calculated by determining the probability of stress exceeding strength.

Whereas the basic analytical procedures in the NGCAD method and the TsAGI method are similar, the detailed treatments of the damage tolerance analysis are significantly different. In the NGCAD approach, a shift factor is applied to the material strength distribution, thereby reducing the average strength by factors accounting for the damage type and size. The factors are determined independently. In the TsAGI approach, the strength reductions are calculated using a two-parameter fracture model for through damages and a sublaminar buckling criterion for a delamination located at the center of the laminate. Strength distributions for the damage strength can be different than for the undamaged laminates. A brief summary of the TsAGI approach follows.

The three types of damage considered in the TsAGI method are surface damage, delamination, and through-thickness damage. The damages are classified as low-velocity impact and moderate-velocity impact. Low-velocity impacts are those that result from ground handling and scheduled maintenance corresponding to impact velocities between 6 to 8 meters per second (20 to 26 feet per second). Moderate-velocity impacts are those that result from impact of ice, concrete piece, stones, hail, bird strikes, uncontained engine failure, etc., and correspond to the impact velocities in the 30 to 200 m/s range (100 to 650 fps). The type and probability of impact depends on the structural location.

An extensive inspection program was conducted by TsAGI to classify the type of damage and the results. Composite structures in MIG-29, SU-27, SU-25, L-1011, and AN-124 airplanes were inspected for impact damage. The results are presented in reference 12 in the form of histograms, making it possible to outline two typical types of damage:

- 5- to 10-mm-diameter damage was detected in wing leading edges, stabilizer skins, actuator fairing skins, and landing gear doors. The damage was caused by impacts from debris during takeoff and landing and classified as moderate-velocity impact.
- 3- to 152-mm-diameter damage occurred during ground maintenance, removal and installation of parts, and operations requiring stepladders.

The results suggest that for skin thicknesses in the range of 1.8 to 3.8 mm (0.07 to 0.15 inch), the size of damage does not depend on skin thickness. The size of damage in sandwich skins (0.5 to 1.0 mm) caused by both low-velocity and moderate-velocity impact corresponds to the size of similar damage in monolithic skins (1.8 to 3.8 mm). These observations were used in reference 12 to derive typical analytical probabilistic laws for composites. The recommended empirical equation for the distribution of damage occurrence has the functional form

$$H(2L) = H_0 \exp(-2L/b) \quad (2)$$

where H_0 and b are empirical constants and $2L$ is the damage diameter. Table 1 shows the data for rate of damage per 1,000 flight hours per square meter, using the constants shown at the top

of the table. Note that the low values of b for group II resulted in steep slopes for that group causing the related curves shown in figure 1 to intersect. The damages are divided into three groups, high, moderate, and low damage rates.

TABLE 1. EMPIRICAL CONSTANTS FOR DAMAGE RATE (Per 1,000 flight hours per square meter)

Group	H_0			b		
	All Damage	Delam.	Hole + Crack	All Damage	Delam.	Hole + Crack
High	3.60	1.60	0.97	38	64	58
Moderate	1.60	0.43	0.81	28	22	27
Low	0.33	0.27	0.13	56	69	55

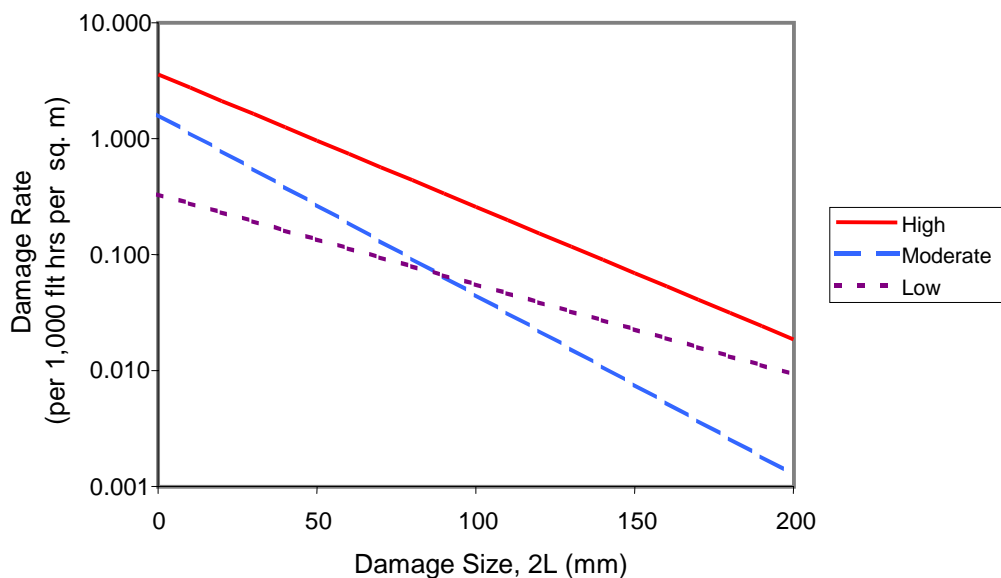


FIGURE 1. EMPIRICAL EXCEEDANCE OF DAMAGE RATE, ALL DATA [12]

As part of the reliability assessment in reference 12, a residual strength analysis was conducted for the damaged composites. Two damage models were considered. A fracture model for composite with through damage at stress concentration and a delamination model.

In addition to the damage modeling, two types of simplified repairs were considered in the probabilistic analysis, airfield repairs and maintenance repairs. The strength restoration factors and their coefficients of variation were used to characterize the reliability of the repair structure.

2.3 NORTHROP GRUMMAN COMMERCIAL AIRCRAFT DIVISION AND TsAGI PROBABALISTIC METHODOLOGIES.

Although the goal of both NGCAD and TsAGI work was to determine the reliability of a composite aircraft component, their approach was quite different. NGCAD method randomly

samples all stochastic variables except material strength and applied load and determines the reliability per flight, R_1 , by a mixed probabilistic method including Monte Carlo simulation and numerical integration. The effect of service life is included by the inclusion of moisture distribution from zero to end of life and cumulative operational damage. The calculated reliability per flight is considered to be an average result in one lifetime if a random sample of aircraft lifetimes is inputted. The reliability for one lifetime, R , is then estimated by the following equation.

$$R = 1 - N * (1 - R_1)$$

where N is the number of flights per life. If the in-service is less than total aircraft life, then the results are interpreted as the average for that segment of service. The results for partial life should not be used to infer lifetime reliability.

TsAGI's methodology treats all variables as occurrences per lifetime. If a damage event is encountered there is a possibility of repair with some strength reduction penalty. Once failure occurs the calculation terminates. At this time moisture and temperature effects are not incorporated into the analysis, but will be in the future. To obtain the probability of failure for one flight, the lifetime probability is divided by the number of flights per lifetime.

The differences and similarities of the TsAGI and the NGCAD methodologies are illustrated in the example problem given in the following subsection.

2.4 EXAMPLE APPLICATION OF THE NGCAD AND TsAGI'S METHODS.

The Lear Fan 2100 composite wing structure was used as a common example problem in references 10 and 12. The analytical model, the input, and analytical approaches are compared in the following paragraphs.

It should be noted that while the DLL for the Lear Fan 2100 was equivalent to an n_z of 3.5, unanticipated failure during static testing of the Lear Fan 2100 occurred at 94% of ultimate load, making it necessary to reduce the DLL to $n_z = 3.29$. In the following discussion, situations corresponding to the reduced load are referred to as the restricted design, while those referring to the full design load are designated the unrestricted design.

2.4.1 Structural Model.

The Lear Fan composite wing structure consists of the upper skin, the lower skin, and the substructures. Both the NGCAD and TsAGI models (figures 2 and 3) apply the same approach by dividing the structure into small panels and computing the probability of failure at the panel level. The NGCAD model employs a detailed model by including all the subpanels in the analysis. The TsAGI model uses a simplified model that includes only the critical panels. As confirmed by the present program, the results of the analyses indicate that the simplified model can obtain the same order of magnitude of failure probability. The number of panels used in the two models is summarized as follows:

- NGCAD Model (figure 2)

Upper wing skin modeled as 5 high strain panels, 16 low strain panels, for a total of 21 panels.
 Lower wing skin modeled as 8 high strain panels, 14 low strain panels, for a total of 22 panels.
 Substructure modeled as 4 high strain panels, 49 low strain panels, for a total of 53 panels.
 Total number of panels in the model is 96.

- TsAGI (figure 3)

Upper wing skin model as 6 high strain panels only.
 Lower wing skin model as 6 high strain panels only.
 Substructure not modeled.
 Total number of panels in the model is 12.

C → Critical										OUTBD
N → Noncritical										
226	198	168	148	128	108	88	69.5	49	28	
U: 20 N L: 42 N	U: 18 N L: 40 N	U: 5 C L: 38 N	U: 15 N L: 36 N	U: 4 C L: 28 C	U: 12 N L: 34 N	U: 3 L: 25,26	U: 9 N L: 32 N	U: 1,2 C L: 22,23 C	U: 6 N L: 30 N	
U: 21 N L: 43 N	U: 19 N L: 41 N	U: 17 N L: 39 N	U: 16 N L: 37 N	U: 14 N L: 29 C	U: 13 N L: 35 N	U: 11 N L: 27	U: 10 N L: 33 N	U: 8 N L: 24 C	U: 7 N L: 31 N	

MODEL AREA = 52 FT² → UPPER,

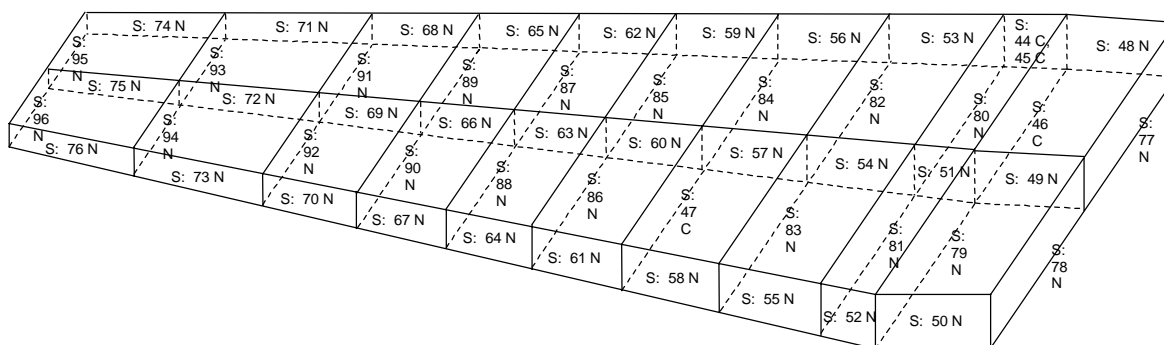


FIGURE 2. NORTHROP GRUMMAN COMMERCIAL AIRCRAFT DIVISION MODEL OF LEAR FAN 2100 WING [10]

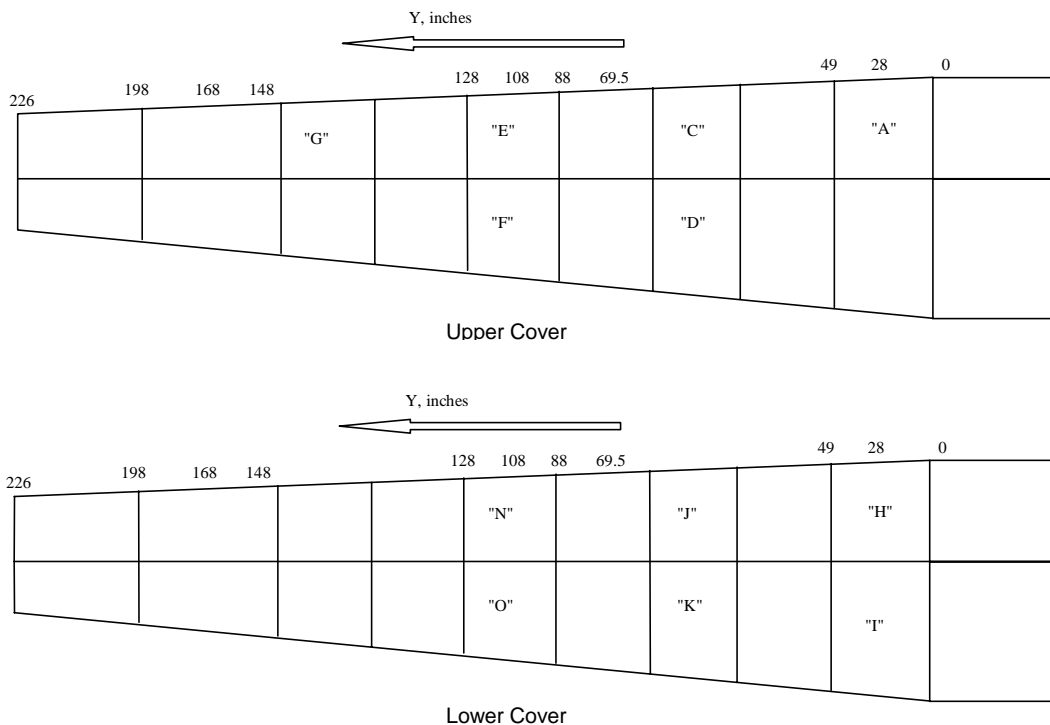


FIGURE 3. CENTRAL AEROHYDRODYNAMIC INSTITUTE MODEL OF LEAR FAN 2100 WING [12]

2.4.2 Load Truncation and Design Factor.

The load truncation factor and the design factor for the two models are as follows:

Load Truncation Factor.

- NGCAD: The probabilistic load distribution is truncated at 150% of DLL.
- TsAGI: Extrapolation of load exceedance curve beyond design limit load.

Design SafetyFactor.

- NGCAD: A conventional factor of safety of 1.50 is used for purposes of scaling the load factors as stresses.
- TsAGI: This factor is not specified but 1.50 is also implied.

2.4.3 Baseline Thickness.

- NGCAD: Two thicknesses are specified. They are 0.2" for upper skin and 0.1" for all locations for moisture consideration.

- TsAGI: Panel thickness is not explicitly used in the model and is not specified.

2.4.4 Surface Area.

The surface area for each panel in the models is given in table 2. As shown in the table, the surface areas in the TsAGI model are, in general, larger than the NGCAD model for critical locations considered. However, because of the different damage tolerance approaches used in the two models, direct comparison of the effects of surface area on the failure probability could not be made.

TABLE 2. COMPARISON OF THE SURFACE AREAS IN THE TWO MODELS

Panel Location		Surface Area (sq. ft.)	
NGCAD (figure 2)	TsAGI (figure 3)	NGCAD	TsAGI
1,2	A	1.35	2.30
3	C	2.20	3.77
4	E	2.15	3.66
5	G	1.88	3.14
11	D	2.64	4.80
14	F	2.36	4.19
22,23	H	1.35	2.30
25,26	J	1.10	3.77
28	N	2.15	3.66
29	O	2.36	4.19
27	K	2.74	3.14
24	I	3.50	3.08
Total		29.58	42.00

2.4.5 Number of $\pm 45^\circ$ Plies.

The influence of the number of $\pm 45^\circ$ plies is more significant in the TsAGI model because the embedded calculations of reduced strength due to damage. The number of $\pm 45^\circ$ plies has no real effect in the NGCAD model since the stress analyses are conducted outside of the probabilistic computations. In fact, this parameter is not needed in the later version of the NGCAD MONTE computer code.

- NGCAD: 7 plies for upper skin, 14 plies for other locations.
- TsAGI: (4/16/4) plies lay-up, (or four 0° plies, sixteen $\pm 45^\circ$ plies, and four 90° plies) in the residual strength example.

2.4.6 Failure Modes.

The NGCAD MONTE code allows up to six failure modes, in the Lear Fan model only two modes are considered. For the TsAGI ProDeCompos code, residual strength analyses were conducted for tension and compression panels based on assumed modes of failure.

- NGCAD considered two failure modes: compression failure in the upper skin and the majority of substructure, and tension failure for lower skin and one panel in the substructure. Environmental degradation of the residual strength is accounted for by a knockdown factor applied to the material strength.
- TsAGI considered two failure modes: buckling failure in the upper skin and tension failure in the lower skin. For the damaged panels, the residual strengths are computed using simple mechanics models described in reference 12. The damage in the upper skin is assumed to be a delamination located at the middle of the skin thickness, while the critical damage in the lower skin is represented as an equivalent circular hole with through-cracks normal to the applied load at the edges of the hole.

2.4.7 Margin of Safety at Critical Locations.

The margins of safety are interpreted differently in the two approaches. In the NGCAD model, M.S. is based on the measured strain from the full-scale static test, adjusted in the restricted design for the reduction to 94% of the DLL, as required in the restricted case (section 2.3). (The full-scale article failed at 94% of ultimate load, therefore mandating the reduction by 6% of the DLL.) For analysis location 1, the measured strain is $-3390 \times 10e^{-6}$ (μ -in/in) while the allowable is -5000μ -in/in, so that the tested M.S. is $-5000/-3390 - 1.0 = 0.47$. For a test factor (factor adjusting the required static load to allow for environmental knockdown of room temperature dry properties; see section 4.3 of reference 10) of 1.14 and a factor of safety of 1.5, the design limit strain becomes $-3390/(1.14*1.5) = -1982$, resulting in an ultimate strain of $1982*1.5 = -2973 \mu$ -in/in; the M.S. is then $-5000/-2973 = 0.68$.

In the TsAGI model on the other hand, a mean failure load factor (MFLF) is computed by first obtaining a margin of safety using the measured strain from the full-scale test for the assumed failure mode (buckling for upper skin and tension failure for lower skin). The allowable used in the computation is a computed value, but the procedure for computing the allowable is not shown in the report. The MFLF is then given by:

$$MFLF = LLF * 1.5 * (M.S. + 1) \quad (3)$$

LLF is the limit load factor which corresponds to 3.29 for the restricted design (section 2.3). Except for locations A, E, and F, the MFLF also includes a scatter factor FB, where $FB = (1 + 1.282 * C_v)$, and C_v is the coefficient of variation of the strength. The value of the C_v is based on engineering judgment in reference 12. Thus, the final MFLF is

$$MFLF = LLF * 1.5 * (M.S. + 1) * (1.0 + 1.282 * C_v) \quad (4)$$

The M.S. computed for the TsAGI model is different from that used in the NGCAD model. A comparison of the M.S. for the associated panel numbers indicated in the TsAGI example and used in NGCAD is shown in table 3.

TABLE 3. COMPARISON OF MARGIN OF SAFETY IN THE TWO MODELS

NGCAD Model		TsAGI Model		NGCAD Model		TsAGI Model	
Location ¹	Point ²	Panel ³	Panel ⁴	M.S. ⁵	M.S. ⁶	MFLF	M.S. ⁷
1, 2	1, 2, 3	A	1	0.68, 1.59	0.68, 1.59, 1.02	5.63	0.14
3	4	C	2	1.02	0.93	9.03	0.68
11	5	D	5	2.00	1.85		0.33
4	6	E	3	0.93	--	5.63	0.14
14	7	F	6	2.00	--	5.63	0.14
5	8	G	4	1.85	--	8.50	0.58
22, 23	23, 24	H	7	1.11, 1.61	1.51, 0.36	10.66	1.11
24	25	I	10	1.36	1.36	12.30	1.37
25, 26	26, 27, 29	J	8	1.36, 1.41	1.41, 1.85, 1.52	11.47	1.21
27	28, 30	K	11	1.85	1.06	14.79	1.85
28	31	N	9	1.06	--	10.64	1.05
29	32	O	12	1.52	--	13.07	1.52

Notes:

1. Panel location as indicated in figure 2.
2. High strain points; see table 4-5 and 4-6 together with figure 4-11 and 4-12 of reference 10 as well as the discussion of p. 4-15 of that reference.
3. Panel designation in figures 17 and 18, reference 12.
4. Panel designation in tables 3 and 4 under comments column, reference 12.
5. M.S. from sample input p. C-3 to C-4, reference 10.
6. M.S. shown in table 4-5 and 4-6, reference 10.
7. M.S. at static test at room temperature dry (RTD) for restricted aircraft (94% of DLL), for tables 3 and 4 of reference 12.

From the above table, the difference in M.S. between the NGCAD and TsAGI analyses is mainly in the upper skin, where the TsAGI values were computed on the basis of buckling failure.

2.4.8 Allowables.

- NGCAD: 5000 μ -in/in strain is used for both tension and compression allowables.
- TsAGI: not specified.

While strain allowables are used in the NGCAD model, allowables are not directly referenced in the TsAGI model. Instead, the TsAGI approach was as follows: residual strength of damaged panels was estimated in the TsAGI analysis from the material properties for the Russian KMU-7 graphite/epoxy. A 24-ply laminate, with a $(\pm 45/90/\pm 45/\pm 45/0/90/\pm 45/0)_s$ lay-up, was assumed together with standard lamination theory and the Tsai-Hill failure criterion, leading to:

Tension:

$$E_x = 5410 \text{ kg/mm}^2 \text{ (7.695 Msi)}$$

$$s_{x,lim} = 21.3 \text{ kg/mm}^2 \text{ (30.3 ksi) for matrix cracking}$$

$$s_{x,ult} = 27.9 \text{ kg/mm}^2 \text{ (39.7 ksi) for fiber failure}$$

$$\epsilon_{x,ult} = 5160 \text{ } \mu\text{-in/in.}$$

Compression:

$$E_x = 5410 \text{ kg/mm}^2 \text{ (7.695 Msi)}$$

$$s_{x,lim} = 21.5 \text{ kg/mm}^2 \text{ (30.6 ksi)}$$

$$s_{x,ult} = 21.9 \text{ kg/mm}^2 \text{ (31.1 ksi)}$$

$$\epsilon_{x,ult} = 4050 \text{ } \mu\text{-in/in.}$$

The upper skin was assumed to be delamination critical. The delamination was assumed to be located at the middle of the skin thickness. The normalized residual strength of the upper skin was then computed and given as a function of delamination size. For the lower skin, crack from a circular hole was assumed to be the critical damage. For a given hole diameter and crack at the edge of the hole perpendicular to the tension load emanating from each side of the hole, the critical tensile stress was determined using a fracture mechanics model. The fracture toughness was assumed to be $85.7 \text{ kg/mm}^{3/2}$. The crack length is determined empirically.

2.4.9 Statistical Distribution of Stresses.

- NGCAD: In references 10 and 11, a lognormal function of the standard form was defined as:

$$g(t) = \frac{1}{(t-t_0)\sqrt{2\pi\sigma}} \exp\left[-\frac{1}{2}\left(\frac{\ln(t-t_0)-\mu}{\sigma}\right)^2\right]$$

where μ and σ , are the mean and standard deviation of the logarithm of the independent variable $(t-t_0)$, and t_0 is the so-called location parameter which defines the lower end of the range for which the distribution applies. The above function found to be suitable for representing the PDF of the load exceedance curve for the Lear Fan 2100 aircraft. Reference 11 gives a procedure which is automated in the form of a Microsoft Excel spreadsheet for developing the lognormal distribution from a known exceedance spectrum. For the upper and lower skins, the three parameter lognormal distribution with parameters $\mu = -0.29634$, $\sigma = 0.53677$, and $t_0 = 2.16$ was used. The 100% design limit stress (DLS) corresponded to the restricted design for which $n_z = 3.29 \text{ g}$, for 1.222 flight hours. For the substructures three parameter lognormal distribution was also used. In this case the parameters were $\mu = -1.06645$, $\sigma = 0.53677$, and $t_0 = 1.00$. The distribution was for 1.222 flight hours and the restricted design case of 3.29 g at 100% DLS.

The probability of gust occurrence is 0.1 with a uniform distribution, and the probability downward gust is 0.0.

- TsAGI: Load spectra were generated from cumulative load exceedance curves Ht as shown in figure 4. The stress distribution is defined by the following equation with a given cumulative load exceedance curve:

$$CDF(x) = \exp[-Ht(x)]$$

For the case of the unrestricted design ($n_z = 3.5$), initial maneuver spectrum exceedance curves from reference 10 were used. The contribution of the gust load was estimated by combining the maneuver load spectrum with the gust load spectrum, taken as statistically independent variables. The gust load spectrum was estimated from similar Russian aircraft of $n_z = 2.9$, the combined gust frequency of exceedance for Lear Fan missions corresponding to nearly 2×10^{-5} per flight hour at $V = 15$ m/s.

For the restricted design ($n_z = 3.29$), the positive load factor of the maneuver exceedance was modified so that the frequency of exceedance of limit load is the same for both the restricted and unrestricted cases. Linear extrapolation on semilogarithmic scale is used for the exceedance curve between limit and ultimate load factors. The typical slope of the exceedance curve for a Russian commercial aircraft is used for extrapolation, see figure 4.

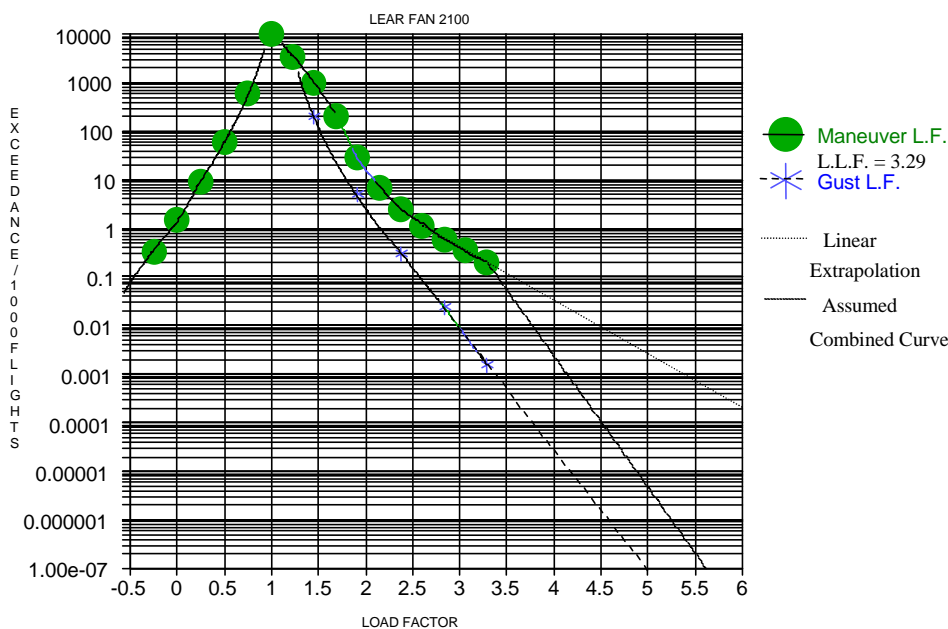


FIGURE 4. EXTRAPOLATED EXCEEDANCE CURVE FOR THE LEAR FAN ANALYSIS

2.4.10 Manufacturing Defects.

- NGCAD: Five types of defects were considered: hole defects, laminate defects, impact induced damage, fiber waviness, and dimensional out-of-tolerance. Defects are described

in terms of rate per unit area and by a strength reduction factor. The probability of occurrence of a defect as described by a Poisson distribution is given by:

$$P(1 \text{ or more defects}) = 1.0 - P(\text{no defect}) \tag{5}$$

Where: $P(\text{no defect}) = \exp(-\text{defect rate} \times \text{surface area})$

As discussed in section 3.6 of reference 11, the latter implies that P(no defect) is governed by a Poisson distribution. Uniform defect rate and constant strength reduction factor were used in the NGCAD example.

- TsAGI: Manufacturing defects and operational damage were combined and expressed in terms of damage frequency of occurrence. Two types of damage were considered: holes with cracks and delaminations. The cumulative number of occurrences per 15,000 flight hours per square meter is given in table 4.

TABLE 4. CUMULATIVE PROBABILITY OF DAMAGE OCCURRENCE
 (Per 15,000 flight hours per square meter)

Damage Size, (CM)	Holes + Cracks	Delamination
0.0	0.2425	0.2435
3.75	0.132	0.219
7.5	0.05	0.146

The residual strength is computed by the method given under the allowables section discussed earlier.

2.4.11 Moisture and Temperature Degradation Effects.

- In the NGCAD analysis the strength reduction due to environment is described as a function of temperature and moisture. The required inputs are time, moisture distribution, thickness, and strength factor. The moisture is expressed as a ratio of the saturated moisture content. The probability of occurrence is computed by assuming a triangular distribution function with minimum, maximum, and density value as 0.0, 1.0, and 0.1.
- The TsAGI analysis did not consider the effects of moisture and temperature.

2.4.12 Operational Defects.

- NGCAD: Three damage types are considered, runway debris, hail, and maintenance induced damage (MID). The required inputs are similar to those for manufacturing defects. A Poisson distribution is again used to compute probability.
- TsAGI: The TsAGI model does not distinguish the manufacturing defects and operational damages (refer to discussion under Manufacturing Defects).

2.4.13 Skin Temperature Distribution.

- NGCAD: Temperature was considered to be a standardized function of altitude and was represented by a histogram of temperature versus altitude using the values shown in table 5. (A similar approach to the effect of temperature is used for the example of the Boeing CX transport discussed in section 3.6.) The statistical distribution of temperatures is generated from this relation of temperature to altitude together with the distribution of times spent at specific altitudes determined by the three assumed mission profiles given in reference 10 for the Lear Fan 2100. All locations on the wing component being analyzed are considered to have same temperature distribution.
- TsAGI: Temperature distribution was not considered in the TsAGI model.

TABLE 5. FLIGHT LIFETIME TEMPERATURE DISTRIBUTION OF THE LEAR FAN 2100 AIRCRAFT [10]

Mean Structure Temperature (°F) in Interval	Time per Lifetime (minutes)	Fraction of Lifetime (%)
-65.5	111,401.4	12.4%
-56.6	4,658.6	0.5%
-47.7	369,769.5	41.1%
-21.0	52,732.1	5.9%
-12.0	47,806.5	5.3%
-3.2	31,621.5	3.5%
2.2	54,197.9	6.0%
14.7	18,625.3	2.1%
23.6	58,526.0	6.5%
32.5	1,468.5	0.2%
37.9	44,359.8	4.9%
55.7	73,622.8	8.2%
100.0	16,454.8	1.8%
160.0	14,740.1	1.6%
Total	899984.5	100.0%

2.4.14 Probability of Damage Detection.

- NGCAD: The probability of damage detection is not considered explicitly in the NGCAD approach.
- TsAGI: The two types of inspection considered are preflight visual and maintenance inspections. The maintenance inspection uses a special method and is applied at 100 flight hour intervals. Based on the TsAGI technique, the probability of detection is given in table 6. The table shows the probability of detection of the two types of damage considered, cracks at holes and delaminations. The upper and lower bound probabilities of detection are curve fits of limited data used in reference 12.

TABLE 6. PROBABILITY OF DAMAGE DETECTION IN THE TsAGI ANALYSIS [12]

Damage Size (cm)	H/C Lower Bound	H/C Upper Bound	Delamination Lower Bound	Delamination Upper Bound
0.0	0.000	0.000	0.000	0.000
1.0	0.008	0.016	0.000	0.006
2.0	0.223	0.552	0.004	0.084
3.0	0.780	0.929	0.020	0.760
4.0	0.914	0.970	0.071	0.913
5.0	0.979	0.991	0.329	0.953
6.0	1.000	1.000	0.690	0.988
7.0	1.000	1.000	0.824	0.999
8.0	1.000	1.000	0.903	1.000
9.0	1.000	1.000	0.948	1.000
10.0	1.000	1.000	0.981	1.000
11.0	1.000	1.000	0.992	1.000
12.0	1.000	1.000	1.000	1.000

Note: H/C denotes holes and cracks.

2.4.15 Repair.

- NGCAD: Repair is not considered.
- TsAGI: The strength restoration and its probabilistic distribution are determined from Russian data for airfield and maintenance repairs. The data are expressed in terms of strength restoration factors and their associated coefficient of variation. The modes of failure for a repaired panel are tension, compression, and buckling.

2.4.16 Comparison of Results.

Analytical results obtained from the two models for single flight probability of failure are compared here. The probabilities of failure are for upper skin (US) and lower skin (LS). Two cases were considered for the upper-skin failure in the NGCAD analyses, buckling and compression. Only tension failure is considered for the lower skin. The NGCAD results include both the restricted and unrestricted aircraft. The comparisons shown in table 7 only include the results of the critical panels (locations).

TABLE 7. COMPARISON OF RESULTS

Analysis Condition	Failure Mode	NGCAD Result	TsAGI Result
Restricted US	Buckling	$1.1409e^{-6}$	$1.47e^{-7}$
Restricted US	Compression	$9.368e^{-10}$	---
Restricted LS	Tension	$1.775e^{-10}$	$6.04e^{-16}$
Unrestricted US	Compression	$1.701e^{-9}$	---
Unrestricted LS	Tension	$2.16e^{-10}$	---

The results in table 7 indicate that direct comparison of the analytical results is difficult because the approaches taken in the two methodologies are significantly different. Even though the two methods both employ Monte Carlo simulation and numerical integration, the input parameters are quite different as delineated in sections 2.4.1 to 2.4.15. For instance, a truncated load distribution is used by NGCAD while TsAGI extrapolates the load exceedance curve past 3.29 g limit load. The NGCAD method assumes an external stress analysis for an undamaged wing with local corrections for stress concentrations at fastener locations, whereas in the TsAGI method, only an embedded stress analysis for the damaged structure is considered in the analysis with no account taken of fastener locations. This could explain the large discrepancy in the results for the tension case.

The TsAGI model resulted in approximately one order of magnitude lower probability of failure in the buckling failure of the upper skin, which is the dominant mode of failure. The TsAGI model does not consider environmental effects but it does include effects of repairs and inspections. Both of these effects would result in higher probability of failure for the NGCAD model, as shown for the buckling failure mode.

In both analyses the probability of tension failure of the lower skin is significantly lower than that for upper-skin buckling.

In conclusion, the example problem illustrates the difficulty of probabilistic analysis. The difficulty is not in mathematical formulation but how the many variables are used in the analysis. Additional complication in the Lear Fan example is that NGCAD and TsAGI approached the problem from different directions. As no finite element analysis was available, the problem existed how to link the loading to the applied stresses in the structure. NGCAD chose to take the failure strains from full-scale test and scale them to the 3.29 g limit load. TsAGI, on the other hand, took the same strains and scaled them to the material allowable and did a simplified stress analysis to link loads to stresses. Thus, there may be some scaling discrepancies between the two analyses.

3. SENSITIVITY STUDIES USING THE NGCAD METHODOLOGY.

An extensive sensitivity study was conducted during the performance of the present program. The parameters considered in the sensitivity study were the number of Monte Carlo simulations, load distribution, manufacturing defects, operational damage, and structural design. The computer code MONTE using the NGCAD methodology was the computational tool used for the sensitivity study. Two structures were analyzed in the study, the Lear Fan wing structure described in references 10 and 11, and the composite wing box tested under the United States Air Force (USAF) Damage Tolerance of Composites program [12]. In addition, two versions of the MONTE code were compared to determine the computational efficiency and accuracy of this method. The results are presented in the following subsections.

3.1 CONVERGENCE OF RESULTS.

In this study, input data used in reference 10 were used to determine the number of Monte Carlo simulations needed to achieve a convergent probability of failure. Results obtained from an

early version of the MONTE code (November 1996) were compared to results obtained from a later version (July 1997). The later version involved:

- Incorporation of closed-form expressions for joint probability distributions for cases involving various combinations of the normal, lognormal and Weibull distributions.
- Adoption of the Romberg integration algorithm [10] for integration of the combined strength and stress distribution corresponding to equation 1.
- Replacement of infinite integration limits by finite limits, based on a choice of limits for which the deviation from the infinite integral gives an error of less than 10^{-40}

The results of the overall structural probability of failure obtained by using the earlier version of the MONTE code are shown in figure 5. The results are plotted as the averaged probability of failure versus the number of Monte Carlo simulations. The averaged probability of failure is the average value of the probability of failure from all simulations. These results indicate that the averaged probability of failure oscillates significantly when the number of simulations is small. The results converged to 9.416×10^{-10} after 190,000 simulations. This value (9.416) is slightly different than table 7, line two, but can be considered identical in this context. From figure 5, the number of Monte Carlo simulations required to achieve a converged probability of failure is approximately 50,000.

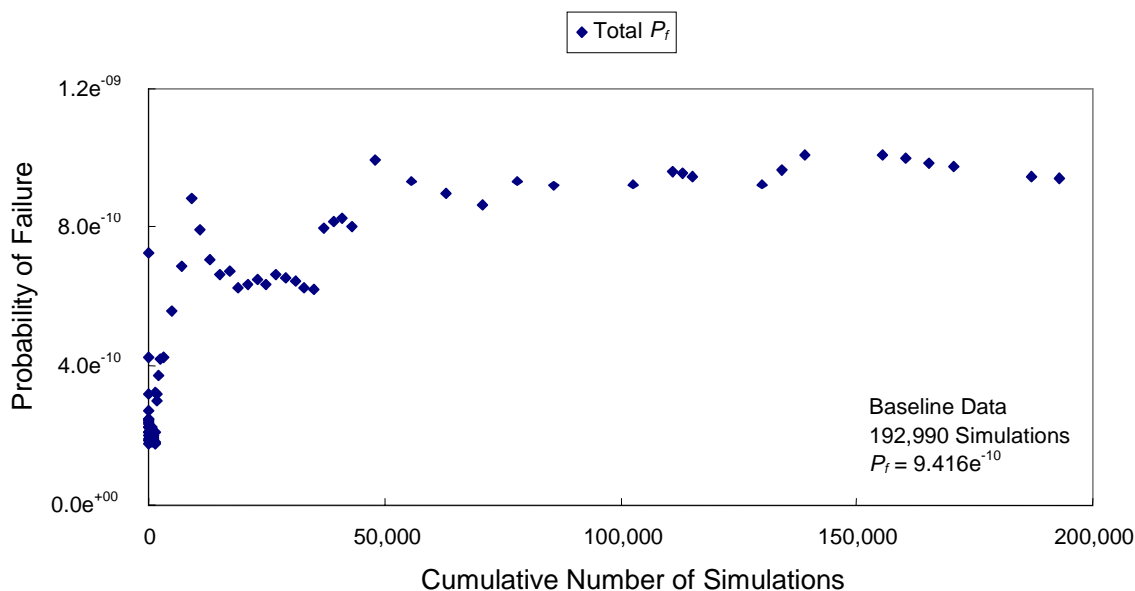


FIGURE 5. AVERAGED OVERALL FAILURE PROBABILITY VERSUS NUMBER OF MONTE CARLO SIMULATIONS

The overall probability of structural failure is usually dominated by a few critical locations in the structure. As in figure 2, in the Lear Fan model the structure is divided into 96 panels and the probability of failure can be categorized by four groups with their values in different orders of magnitude. The most critical group consists of the most critical locations. (In the following

discussion, location refers to the panel numbers in the upper part of figure 2; e.g., location 1 refers to the upper-skin leading-edge panel in the second row spanwise from the root end of the wing.) Results show that location 1 has the highest failure probability, as shown in figure 6, in terms of the number of Monte Carlo simulations. The probability of failure at this location is on the same order of magnitude, 10^{-10} , as the probability of failure for the overall structure, shown in figure 5. For the panels in Group 2 the probabilities of failure are in the order of 10^{-11} . These locations do effect the overall structural failure to some extent, but are secondary in importance to the Group 1 elements. The results for the Group 2 panels are shown in figure 7. In the case of the Group 3 panels, their probability of failure (figure 8) is on the order of 10^{-12} and their influence in the overall structural failure is very small. The results for Group 4 (figure 9) are on the order of 10^{-13} or lower which have negligible effect.

In figures 6 to 9, the variables rank, location, and P_f denote the rank of failure probability in descending order, location identification in the analysis model, and the weighted average probability of failure at the location, respectively. Only results for the critical locations are shown in these figures. The location identification refers to the panel number shown in figure 2.

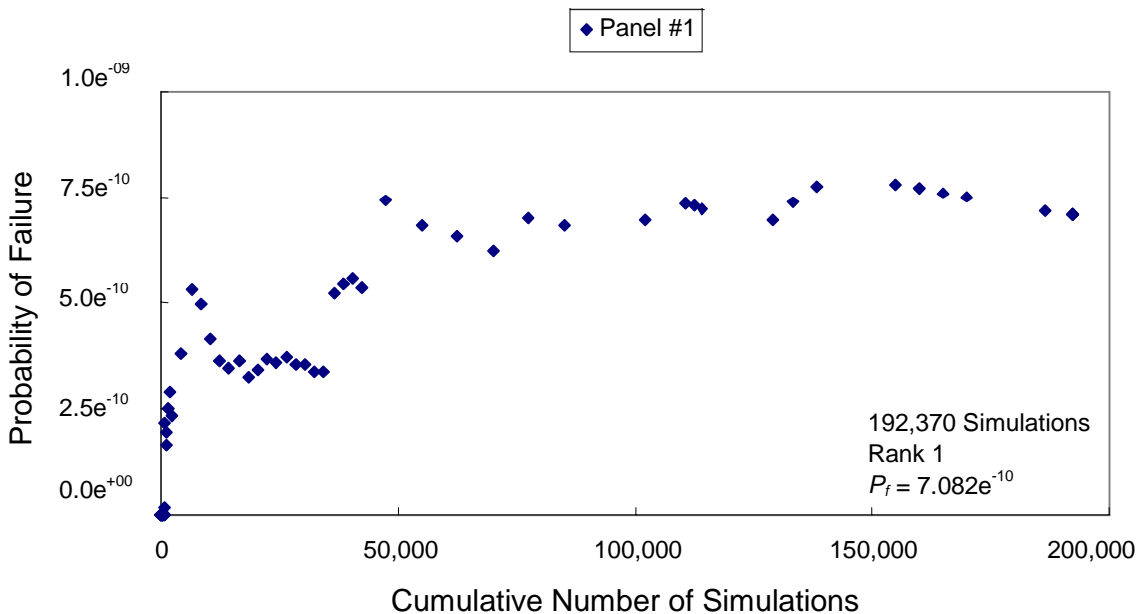


FIGURE 6. AVERAGE PROBABILITY OF FAILURE AT THE MOST CRITICAL LOCATION (panel 1 of figure 2)

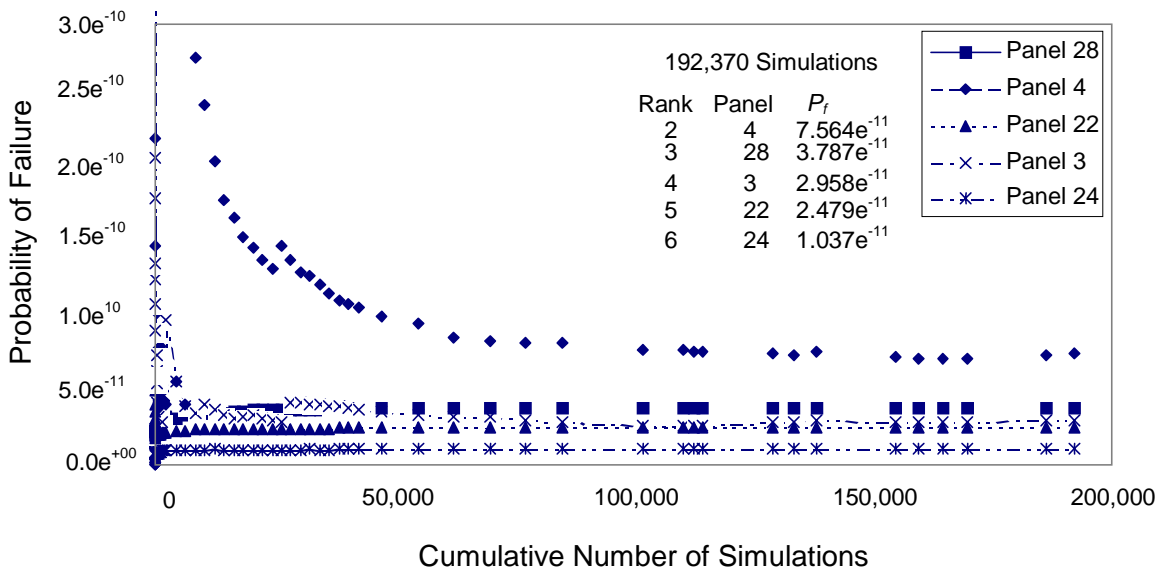


FIGURE 7. AVERAGE PROBABILITY OF FAILURE FOR GROUP 2 PANELS

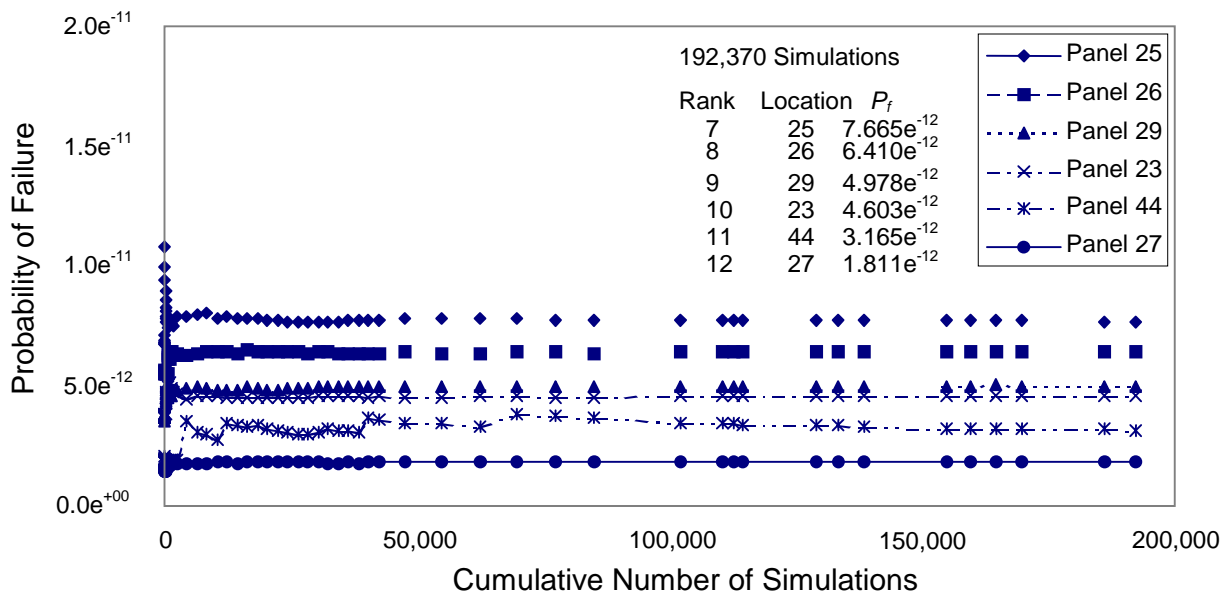


FIGURE 8. AVERAGE PROBABILITY OF FAILURE FOR GROUP 3 PANELS

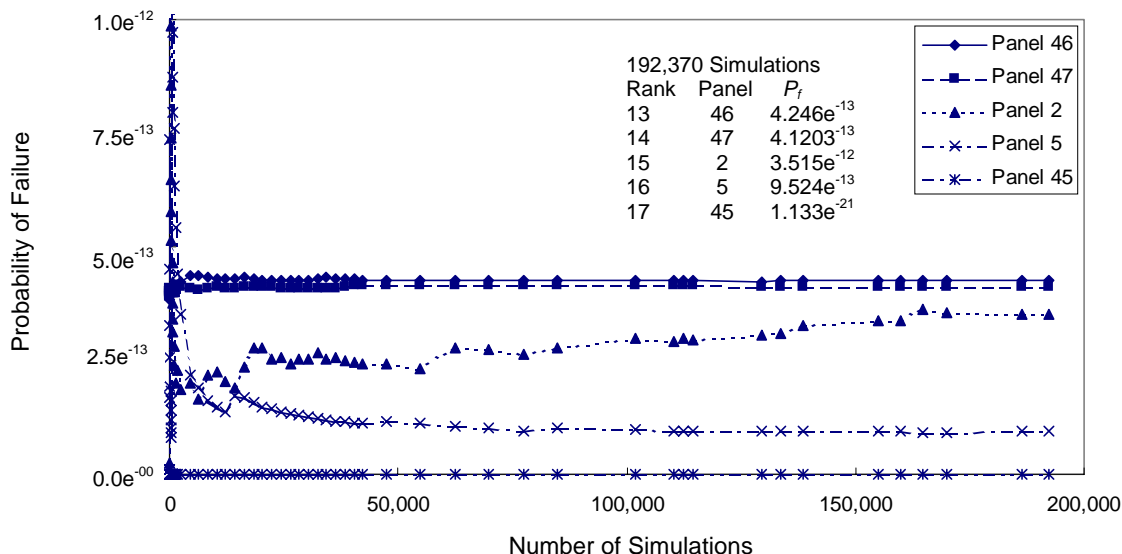


FIGURE 9. AVERAGE PROBABILITY OF FAILURE FOR GROUP 4 PANELS

Because of the long execution time required in the MONTE code, especially for structural models with large numbers of locations, a study was conducted to determine the number of Monte Carlo simulations needed to approximate an estimate of the failure probabilities. Table 8 summarizes the number of Monte Carlo simulations required to obtain results within $\pm 10\%$ of the converged failure probability for each location in the Lear Fan wing model (figure 2).

The results shown in table 8 indicate that the number of simulations required varies with panel location corresponding to the predicted failure probability. Even though 50,000 simulations provide a good approximation for the overall failure probability for the structure, this does not assure that all locations in the structure achieved a stabilized failure probability for that number of simulations. For the structure considered, 140,000 simulations will assure that the failure probabilities have converged within $\pm 10\%$ at every location.

As noted previously, the later version of the MONTE code used more efficient numerical schemes, which significantly reduced the computing time. The difference in computing time is attributed to the shorter integration intervals used in the new version. The overall structural failure probabilities for the structure as a whole obtained with the later version are shown in figures 10 to 12. The weighted average referred to in these figures is the average probability weighted by the number of Monte Carlo simulations in each computer run (not the average probability from the results of computer runs). Thus, if P_{fi} is the probability of failure in the i th computer run with N_i Monte Carlo simulations, then the weighted average of failure probability for a total of M runs is given by

$$P_f = \frac{\sum_{i=1}^M N_i P_{fi}}{\sum_{i=1}^M N_i}$$

TABLE 8. NUMBER OF MONTE CARLO SIMULATIONS FOR APPROXIMATE PROBABILITY OF FAILURE (“Location” refers to panel number of figure 2)

Location	P_f	$\pm 10\% P_f$	No. of Simulations
All	$9.416e^{-10}$	8.560 – 10.358	47,990
1	$7.082e^{-10}$	6.438 – 7.790	77,370
4	$7.564e^{-11}$	6.876 – 8.320	77,370
28	$3.787e^{-11}$	3.443 – 4.166	8,370
3	$2.958e^{-11}$	2.689 – 3.254	129,370
22	$2.479e^{-11}$	2.253 – 2.726	4,370
24	$1.037e^{-11}$	0.943 – 1.141	4,370
25	$7.665e^{-12}$	6.968 – 8.432	300
26	$6.410e^{-12}$	5.827 – 7.051	630
29	$4.978e^{-12}$	4.525 – 5.475	630
23	$4.603e^{-12}$	4.184 – 5.063	1,470
44	$3.165e^{-12}$	2.877 – 3.481	101,870
27	$1.811e^{-12}$	1.646 – 1.992	970
46	$4.246e^{-13}$	3.860 – 4.671	50
47	$4.120e^{-13}$	3.746 – 4.532	10
2	$3.515e^{-13}$	3.195 – 3.866	138,620
5	$9.524e^{-14}$	8.658 – 10.476	62,370
45	$1.133e^{-21}$	1.030 – 1.246	69,870

Figure 10 shows the results of 100,000 Monte Carlo simulations in terms of 100 sets of simulations with 1000 Monte Carlo simulations in each set. The figure shows that the maximum probability of failure is $5.84e^{-09}$ and the overall average failure probability is $4.374e^{-10}$. The absolute value of the average failure probability is different from the results obtained from the earlier version of the code, but the same order of magnitude.

The results shown in figures 11 and 12 indicate trends that are similar to those shown in figure 10. Figure 11 gives the results for 100 sets using 5000 Monte Carlo simulations, for each set, for a total of 500,000 Monte Carlo simulations. This gives a maximum predicted failure probability of $2.090e^{-09}$ with an overall average of $4.427e^{-10}$. Note that these values agree satisfactorily with those shown in figure 10.

Figure 12 shows the results obtained by combining the results incorporated in figures 10 and 11 corresponding to a total of 600,000 simulations, with an additional 49 sets of 10,000 simulations each, corresponding to 490,000 Monte Carlo simulations for a grand total of 1,090,000 Monte Carlo simulations. Figure 12 again shows failure probabilities, which are similar to those in the previous figures. The overall maximum failure probability is $5.843e^{-09}$ (outside the range of the plotted area), and the overall average is $4.258e^{-10}$. The results in figure 12 indicate that the number of Monte Carlo simulations required to obtain results within $\pm 10\%$ is approximately 420,000.

Monte 7/16/97 Version, set of 1000 Monte Carlo Simulations

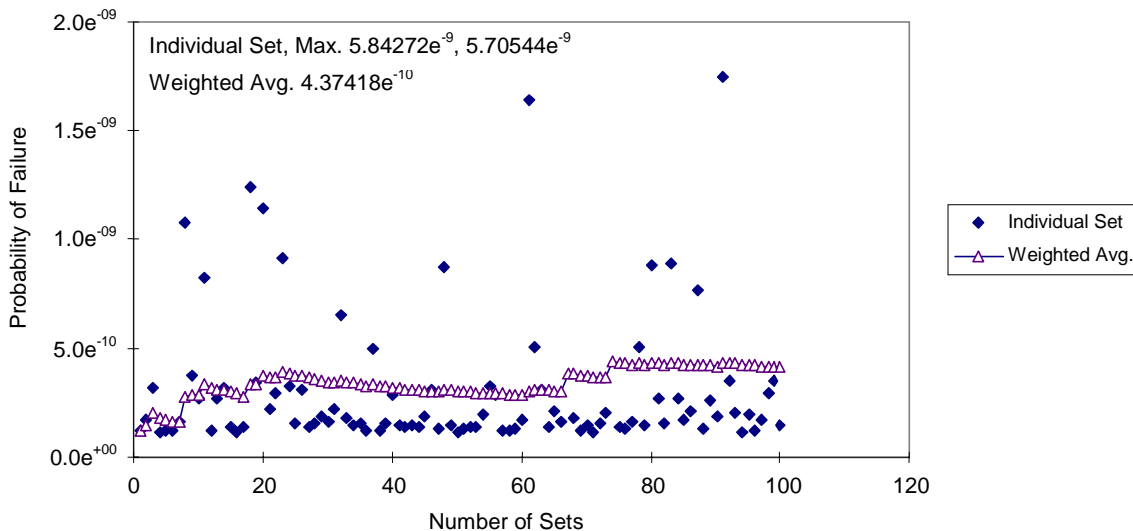


FIGURE 10. AVERAGE PROBABILITY OF FAILURE FOR THE OVERALL LEAR FAN MODEL, BASED ON 1000 SIMULATIONS IN EACH SET

MONTE 7/17/97 Version, Set of 5000 MC

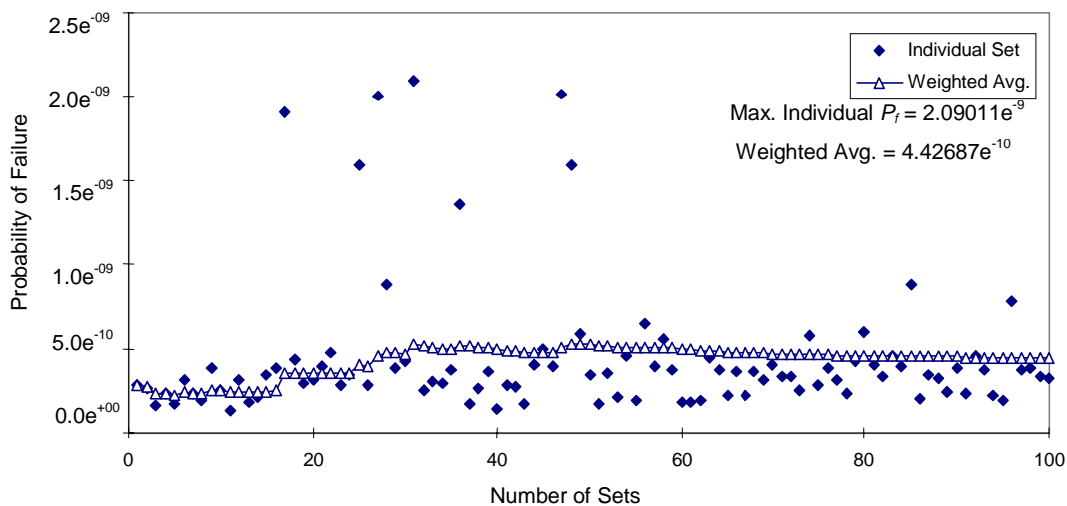


FIGURE 11. AVERAGE PROBABILITY OF FAILURE FOR THE OVERALL LEAR FAN MODEL, BASED ON 5000 SIMULATIONS IN EACH SET

Monte Carlo Simulation Summary

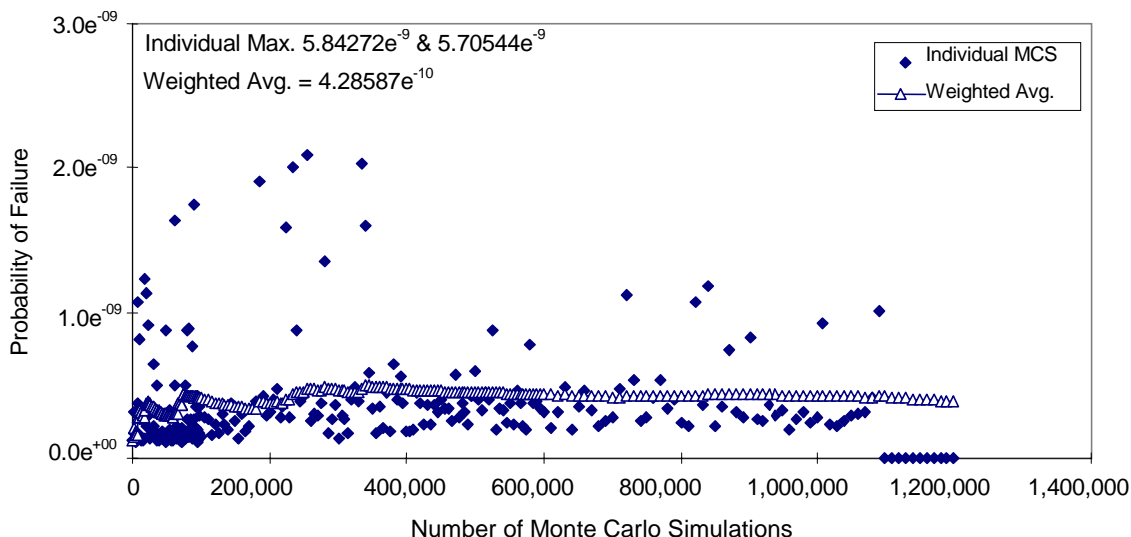


FIGURE 12. AVERAGE PROBABILITY OF FAILURE FOR THE OVERALL LEAR FAN MODEL, COMBINED RESULTS

3.2 SENSITIVITY OF LOAD DISTRIBUTION FUNCTION.

As discussed in section 2.4.9, the PDF assumed for the distribution of peak load factors in the Lear Fan composite wing model was a three-parameter lognormal distribution. The baseline parameters for the skins and substructures are given in table 9 and the PDFs are shown in figure 13.

TABLE 9. PARAMETERS FOR THE LOAD FACTOR DSITRIBUTION

Type PDF	Skin Lognormal	Substructure Lognormal
μ	-0.29634	-1.06645
σ	0.53677	0.53677
t	2.16	1.0

As in section 2.4.9, the lognormal PDF is given by the expression:

$$g(t) = \frac{1}{(t-t_o)\sqrt{2\pi\sigma}} \exp\left[-\frac{1}{2}\left(\frac{\ln(t-t_o)-\mu}{\sigma}\right)^2\right] \quad (6)$$

where μ is the mean and σ is the standard deviation of $\ln(t-t_o)$; t_o is a shift factor.

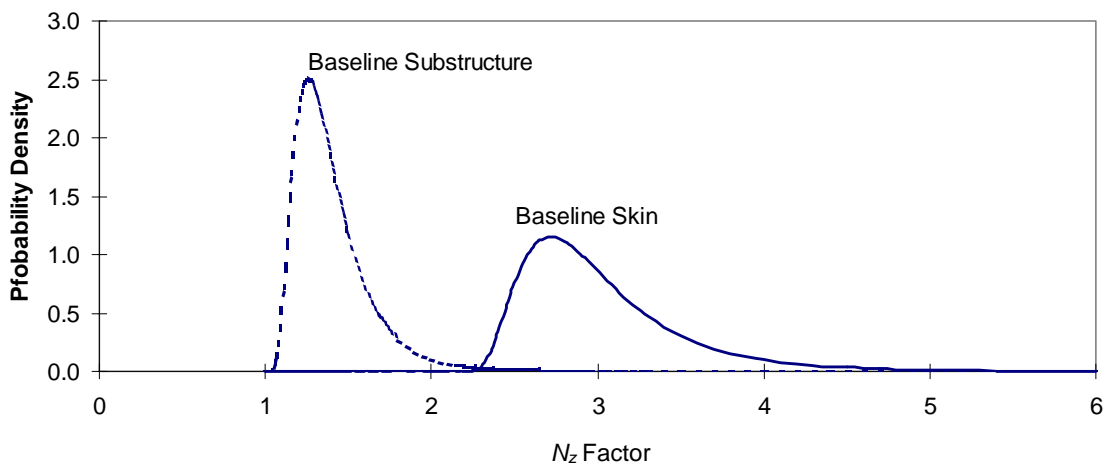


FIGURE 13. BASELINE PDFs FOR THE LEAR FAN WING SKINS AND SUBSTRUCTURES

Parametric studies were conducted to evaluate the effects of mean, standard deviation, and shift factor on the failure probability of the structure. To investigate the effects of the logarithmic mean of the distribution, it was varied from -0.25 to -0.40 for the skin-load factor with the baseline mean approximately in the middle of this range. The scatter range of the load PDFs is shown in figure 14, while the overall structural failure probability obtained from Monte Carlo simulation is shown in figure 15.

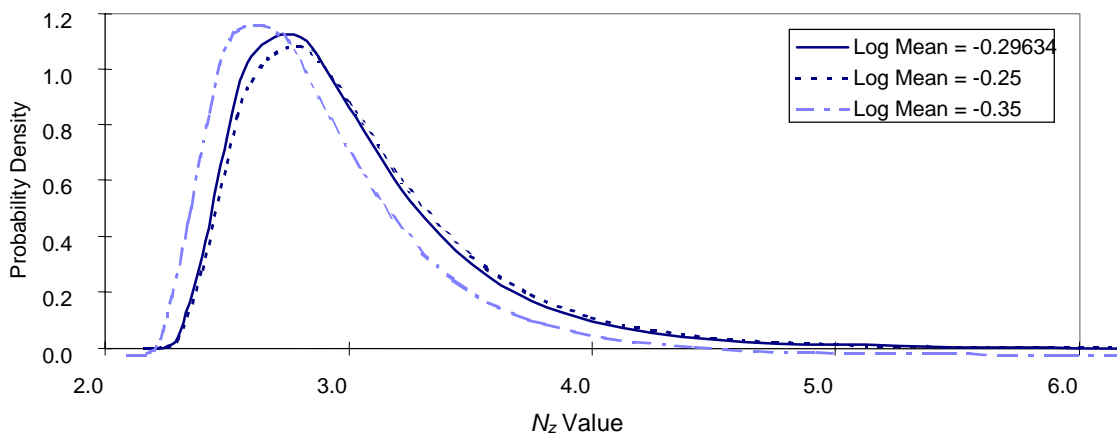


FIGURE 14. WING SKIN LOAD FACTOR PDF WITH VARIABLE LOG MEANS

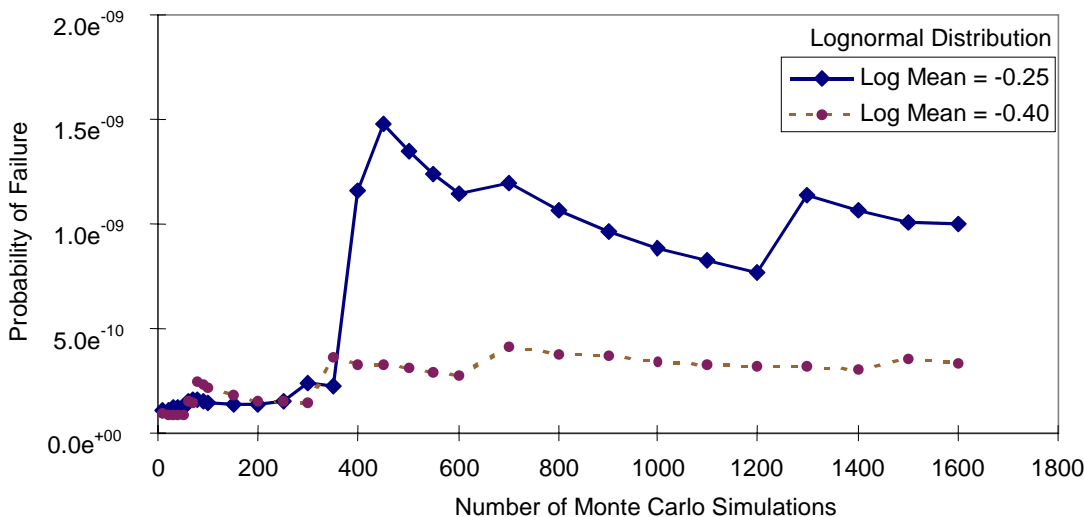


FIGURE 15. EFFECTS OF LOAD FACTOR DISTRIBUTION MEAN ON THE OVERALL PROBABILITY OF FAILURE

Fully convergent results for this load parameter sensitivity study were not obtained. These results are used only to illustrate the effects of the selected parameters on the failure probability of the structure and not to determine their actual values. The results shown in figure 15 confirm, however, that the overall structural failure probability increased with increasing the log mean value, that is, with increasing mean load factor.

The effect of scatter of the load factor distribution on the failure probability was evaluated by varying the σ parameter of the log normal distribution from 0.5 to 0.7. The PDFs of these load factor distributions are shown in figure 16 and the predicted failure probabilities are given in figure 17.

The results in figure 17 show that the overall probability of failure increases with increasing value of standard deviation. This is to be expected, based on the distributions shown in figure 16. Even though the results in figure 17 show that the probability of failure is not fully converged with the limited number of simulations conducted in the analysis, the trend in terms of the standard deviation is clearly established.

The effects of the shift parameter in the lognormal distribution were evaluated by varying the value of t from 1.5 to 2.0. The load factor distributions are shown in figure 18 and the predicted failure probability results are plotted in figure 19.

Figure 19 shows that the failure probability increases with increasing shift factor. Similar failure probability was obtained for $t_o = 1.50$ and $t_o = 1.75$ for a limited number of simulations. The probability of failure increased significantly when the shift factor changed from 1.75 to 2.0.

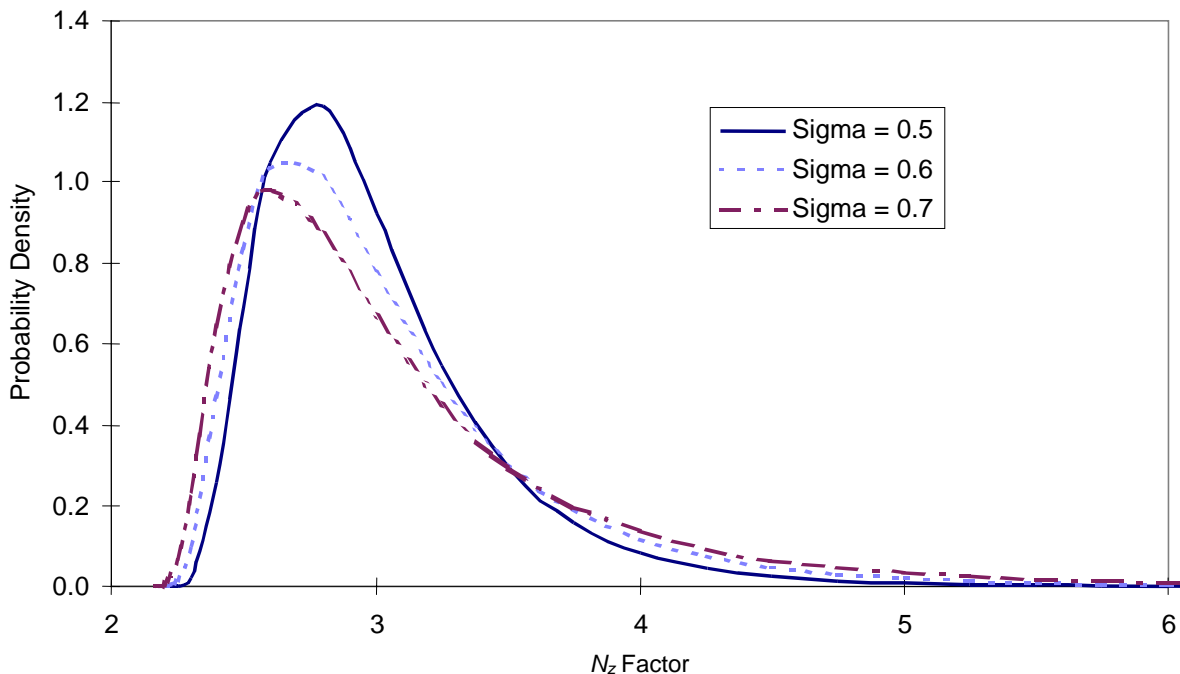


FIGURE 16. WING SKIN LOAD FACTOR PDF WITH VARIABLE σ

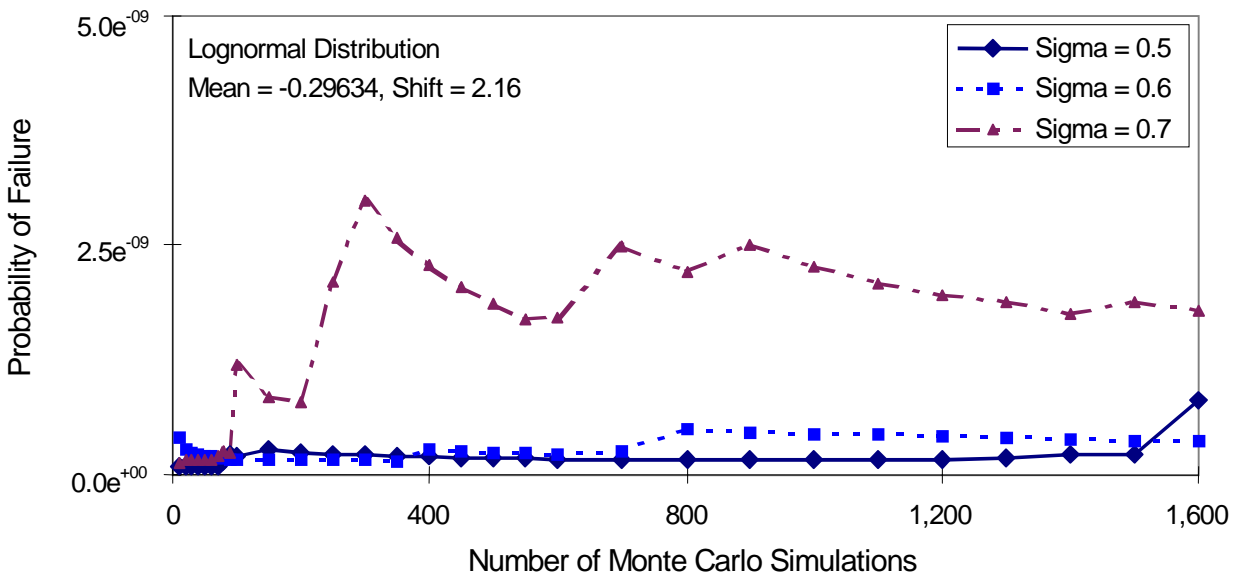


FIGURE 17. EFFECTS OF LOAD FACTOR DISTRIBUTION σ ON THE OVERALL PROBABILITY OF FAILURE

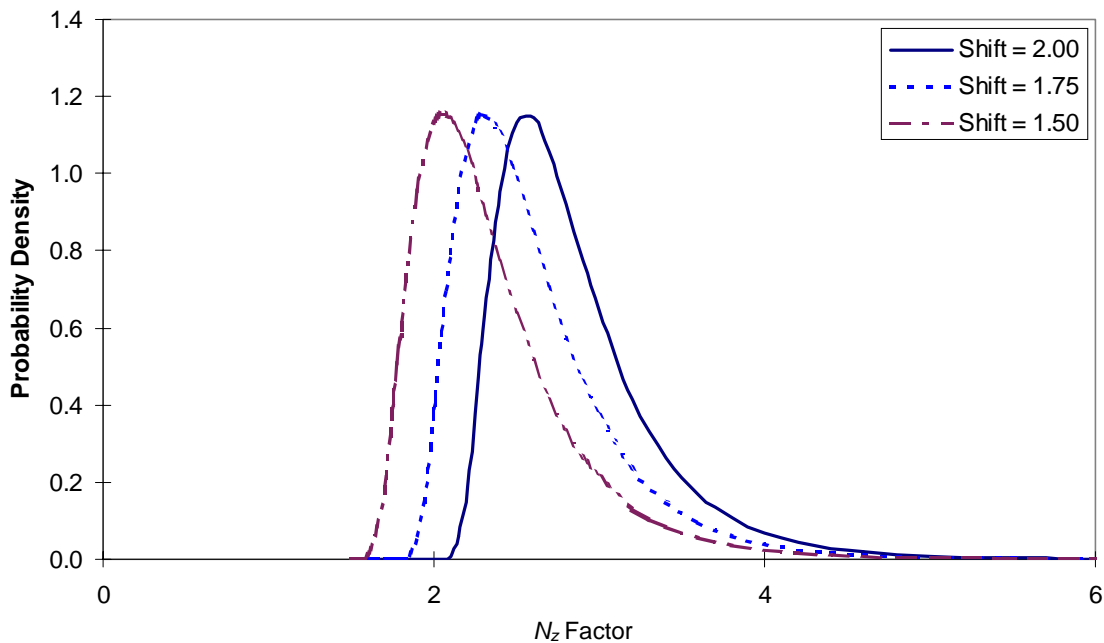


FIGURE 18. SKIN LOAD FACTOR DISTRIBUTIONS WITH VARIABLE SHIFT FACTOR IN THE LOGNORMAL DISTRIBUTION

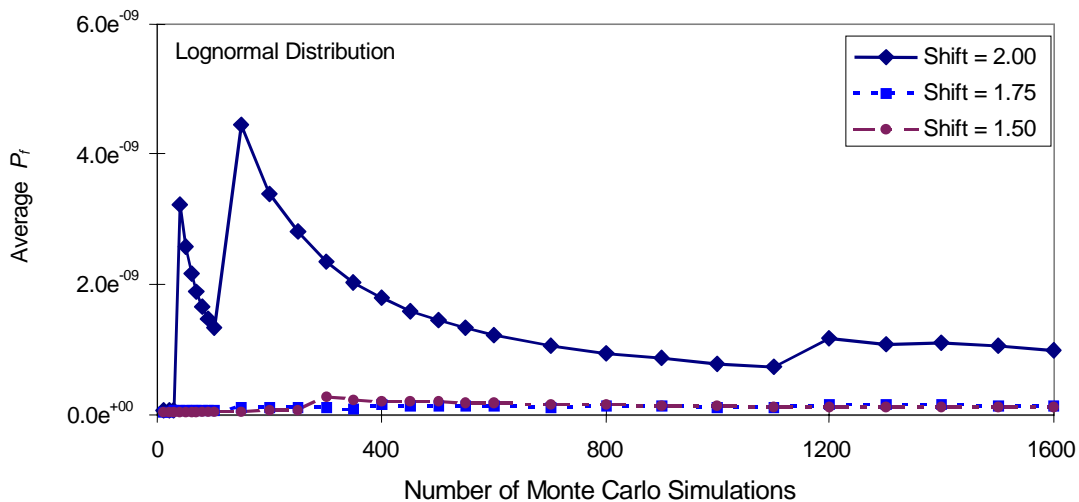


FIGURE 19. EFFECTS OF LOAD DISTRIBUTION SHIFT FACTOR ON THE FAILURE PROBABILITY

In summary, the effects of the load distribution parameters on failure probability follow the same trend as these factors on the load distribution itself. That is, the probability of structural failure increases as the load increases. However, because of the randomness of the variables, accurate functional relationship between the load distribution parameters and the failure probability can not be established explicitly.

3.3 SENSITIVITY OF OPERATIONAL DAMAGE PARAMETERS.

Three types of operational damage were considered in the NGCAD methodology, impact by runway debris, hail impact, and MID. The parameters used in the MONTE code to evaluate the effects of damage include the impact rate per square foot of structural area per flight hour of operation (R_o) and strength reduction factors (FT for tension, FC for compression). The baseline MID parameters are $R_o = 8.00e^{-09}$ per ft², $FC_o = 0.57$ and $FT_o = 0.67$. The subscript o refers to operational damage. Sensitivity studies were conducted to evaluate the effects of damage rate and strength factor on the failure probability. The value of the damage rate considered in the sensitivity study ranged from $8.00e^{-09}$ to $1.00e^{-06}$ for the wing skins. The strength reduction factor for the compression skin, (upper wing skin), was varied in the study from 0.3 to 0.7, whereas the tension skin (lower wing skin) strength reduction factor was assumed uniform at 0.67. The study concentrated on the upper skin because compressive residual strength is more sensitive to impact damage than tension strength. Another reason for selecting the upper skin was that the most critical location, in terms of failure probability, was in the upper skin as discussed in section 3.2 (see table 8).

The failure probabilities (P_f) after 110,000 Monte Carlo simulations are given in table 10 for different values of R_o , with constant FT_o and FC_o . Figures 20 to 24 show the overall failure probabilities and the results are summarized in figure 25.

TABLE 10. EFFECTS OF MID DAMAGE RATE ON FAILURE PROBABILITY

Damage Rate R_o , flt hr ⁻¹ ft ⁻²	Max. P_f	Min. P_f	Average P_f
$1.00e^{-08}$	$1.010e^{-09}$	$2.191e^{-10}$	$3.843e^{-10}$
$2.00e^{-08}$	$1.274e^{-09}$	$2.025e^{-10}$	$4.719e^{-10}$
$5.00e^{-08}$	$3.834e^{-10}$	$2.017e^{-10}$	$2.986e^{-10}$
$1.00e^{-07}$	$9.245e^{-10}$	$2.502e^{-10}$	$3.789e^{-10}$
$1.00e^{-06}$	$1.434e^{-09}$	$5.265e^{-10}$	$7.272e^{-10}$

Notes: 110,000 Monte Carlo simulations.
 Damage rates above are for the compression skin.
 $FT_o = 0.67$, $FC_o = 0.57$.

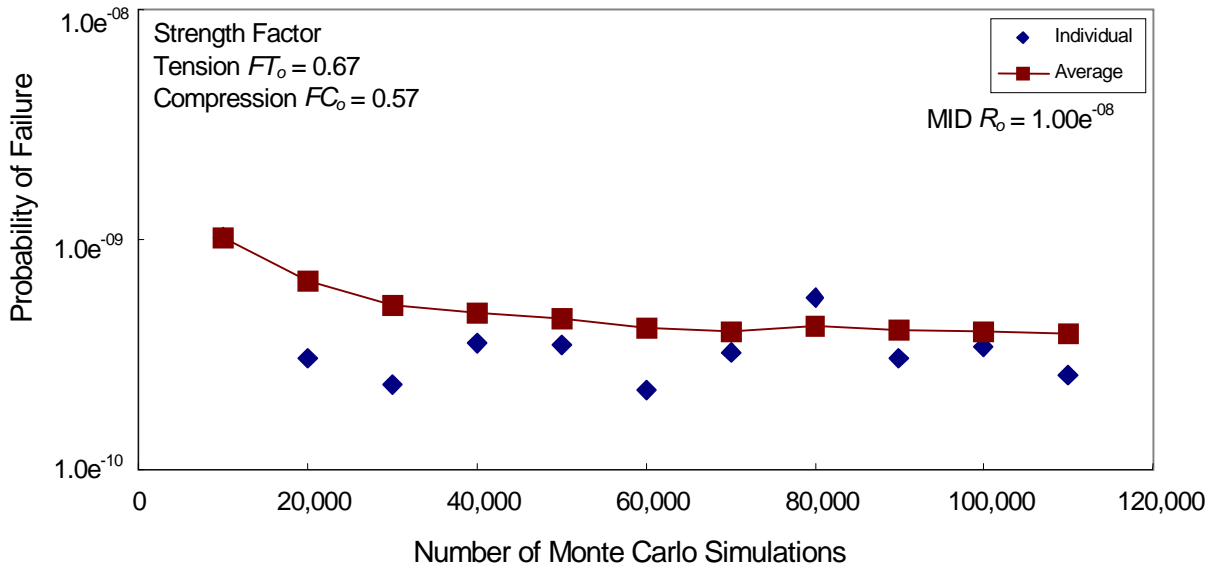


FIGURE 20. OVERALL P_f FOR $R_o = 1.00e^{-08}$

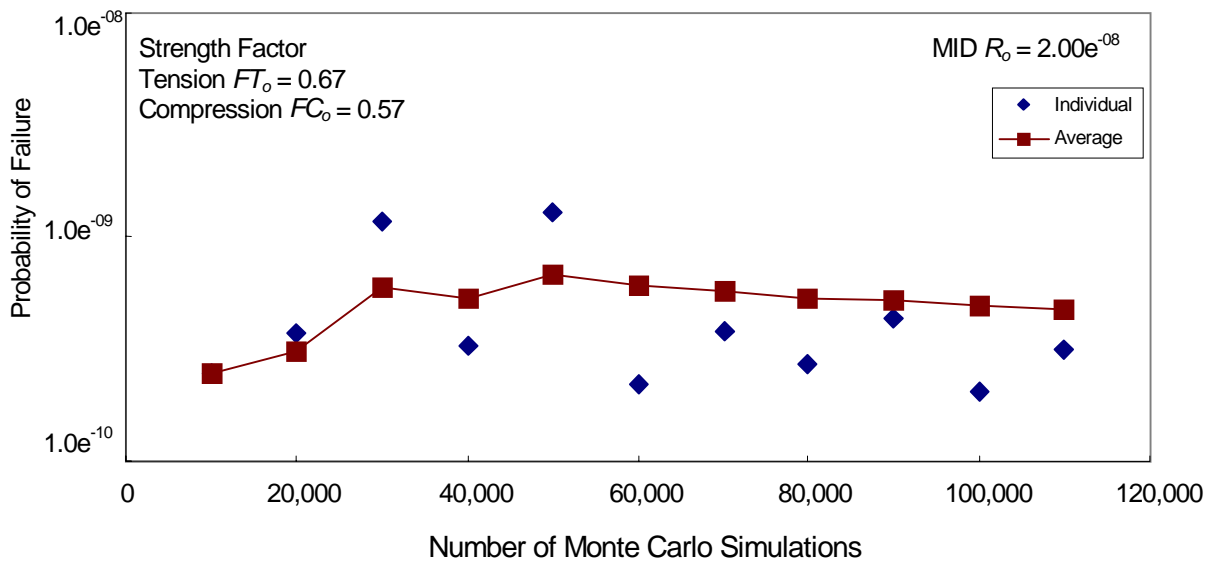


FIGURE 21. OVERALL P_f FOR $R_o = 2.00e^{-08}$

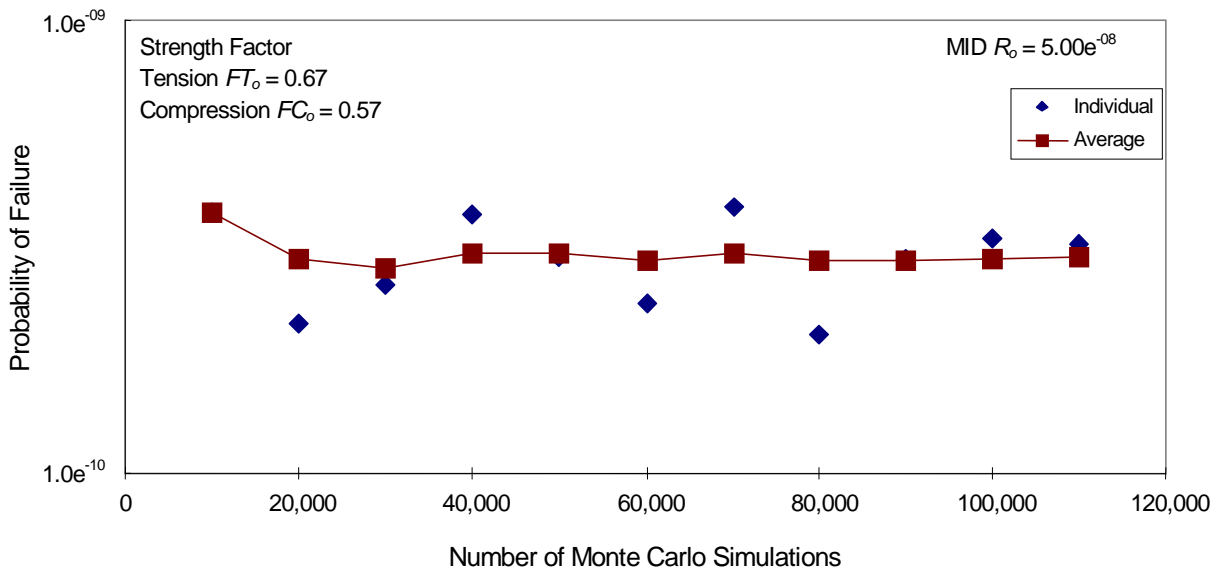


FIGURE 22. OVERALL P_f FOR $R_o = 5.00e^{-08}$

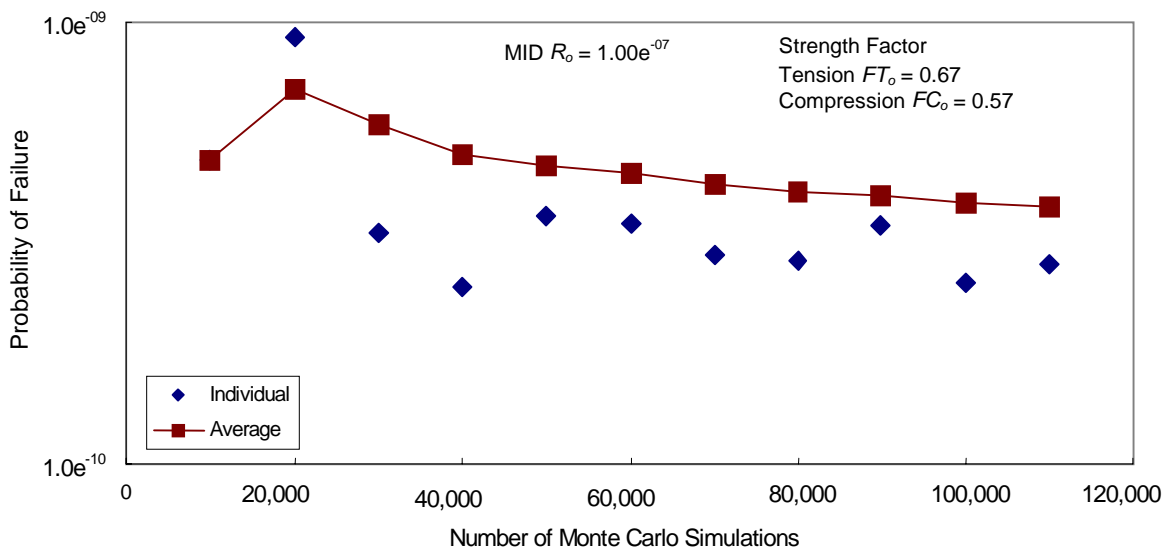


FIGURE 23. OVERALL P_f FOR $R_o = 1.00e^{-07}$

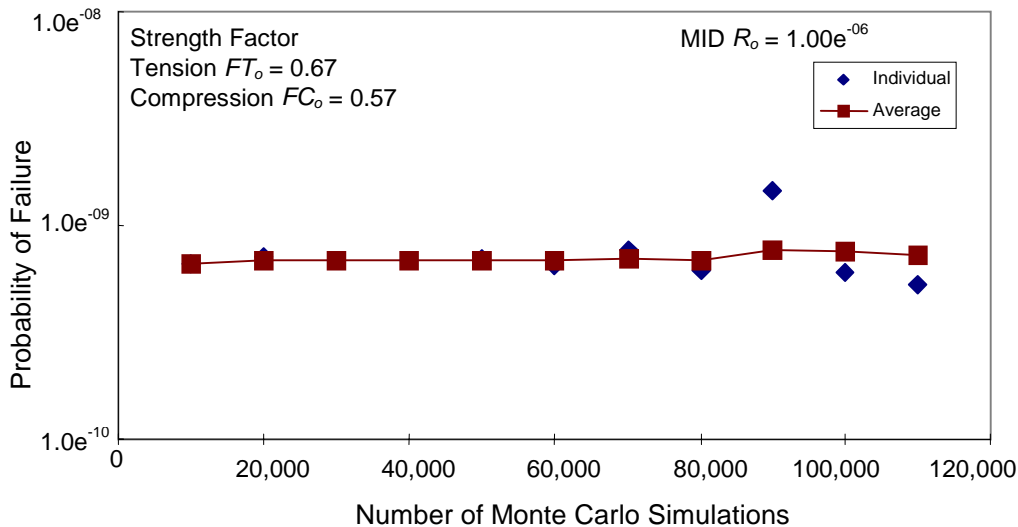


FIGURE 24. OVERALL P_f FOR $R_o = 1.00e^{-06}$

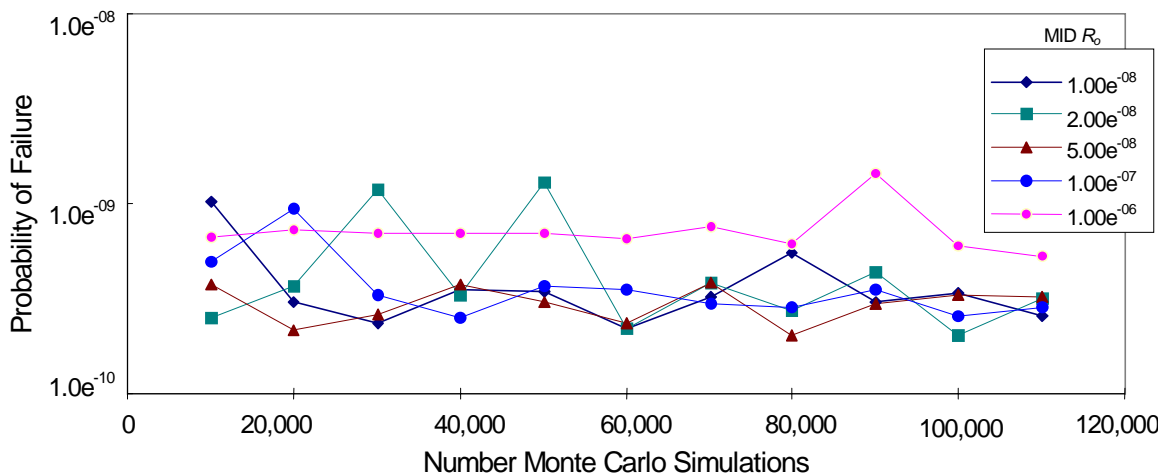


FIGURE 25. SENSITIVITY OF THE OVERALL FAILURE PROBABILITY TO UPPER SKIN MID RATE

The results in figures 20 to 25 show that with a two orders of magnitude change in the value of damage rate, there is no significant change in the overall probability of failure of the structure. These results also confirm an earlier observation that 100,000 Monte Carlo simulations may provide a good approximation for the overall structural P_f although a larger number of simulations are needed for full convergence of the results.

The effects of the compressive strength reduction factor (FC_o) were also evaluated. The structural failure probability is more significantly affected by the FC_o . With FT_o at a constant of 0.67 and R_o for the substructure of $8.0e^{-09}$ ft², the overall structural P_f is summarized in table 11 and plotted in figure 26. All results are based on 110,000 Monte Carlo simulations.

TABLE 11. EFFECTS OF COMPRESSIVE STRENGTH REDUCTION FACTOR FROM OPERATIONAL DAMAGE ON P_f

SKIN R_o	FC_o	P_f
$8.00e^{-09}$	0.3	$1.1126e^{-07}$
$8.00e^{-09}$	0.5	$4.3613e^{-10}$
$8.00e^{-09}$	0.7	$3.4604e^{-10}$
$1.00e^{-06}$	0.3	$1.8042e^{-05}$
$1.00e^{-06}$	0.5	$2.6297e^{-09}$
$1.00e^{-06}$	0.7	$4.8909e^{-10}$

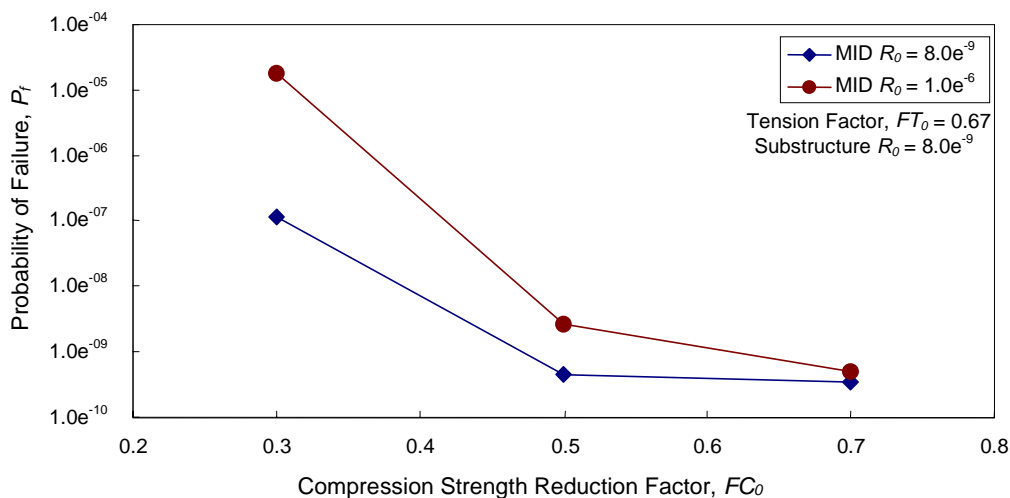


FIGURE 26. EFFECTS OF OPERATIONAL DAMAGE PARAMETER FC_o ON P_f

As shown in figure 26 and table 11, P_f is significantly affected by FC_o while the other damage parameters are held constant. With FC_o changed from 0.7 to 0.3 and the value of R_o increased by three to four orders of magnitude, figure 26 also confirms that the effect of R_o on P_f is secondary for FC_o less than 0.5. For small FC_o , the effect of R_o is significant. It should be noted that section 3.3 investigated the effect of R_o for $FC_o = 0.57$. If FC_o was made smaller, i.e., 0.3, there is an interaction that was not discovered by the specific sensitivity study that was performed in section 3.3.

The value of FC_o also changes the relative probability of failure at different locations in the structure. This is because the upper skin becomes more critical for lower values of FC_o . Three specific locations in the structure were selected for a relative failure probability study. They were Locations 1 and 4, the most critical locations on the upper skin, and Location 28, the most critical location on the lower skin (see figure 2). The relative P_f in terms of percent of overall P_f for Locations 1, 4, and 28 are shown in figure 27 to 29. These figures show results for $FT_o = 0.67$, $FC_o = 0.57$, and variable R_o . As shown in these figures, because the values of FT_o and FC_o are constants, the relative P_f are not significantly changed. Location 1 dominates the failure probability with approximately 50% to 70% of the overall P_f . The relative P_f for Location 4 ranges from 5% to 8%, and for Location 28 it is from 7% to 13%.

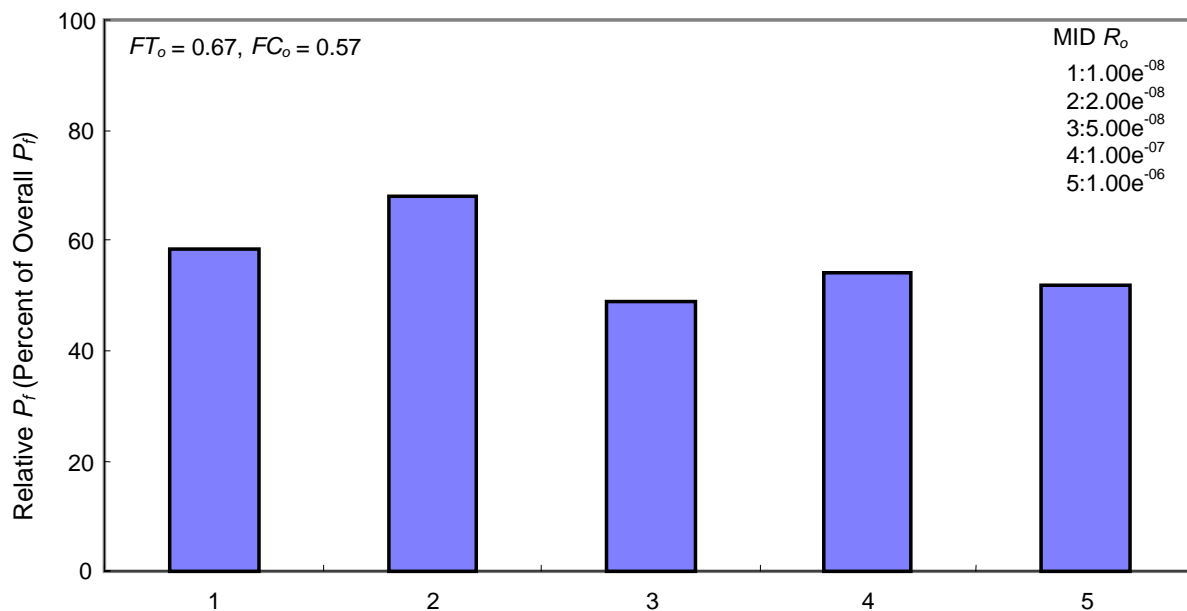


FIGURE 27. RELATIVE P_f FOR LOCATION 1 WITH VARIABLE R_o FOR MID

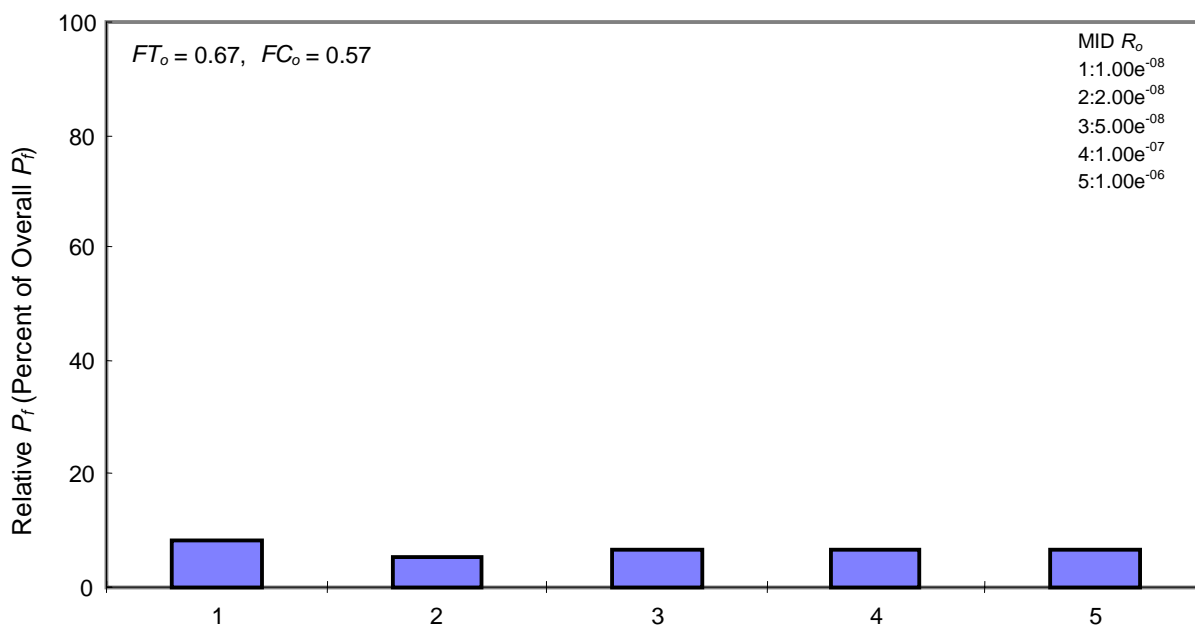


FIGURE 28. RELATIVE P_f FOR LOCATION 4 WITH VARIABLE R_o FOR MID

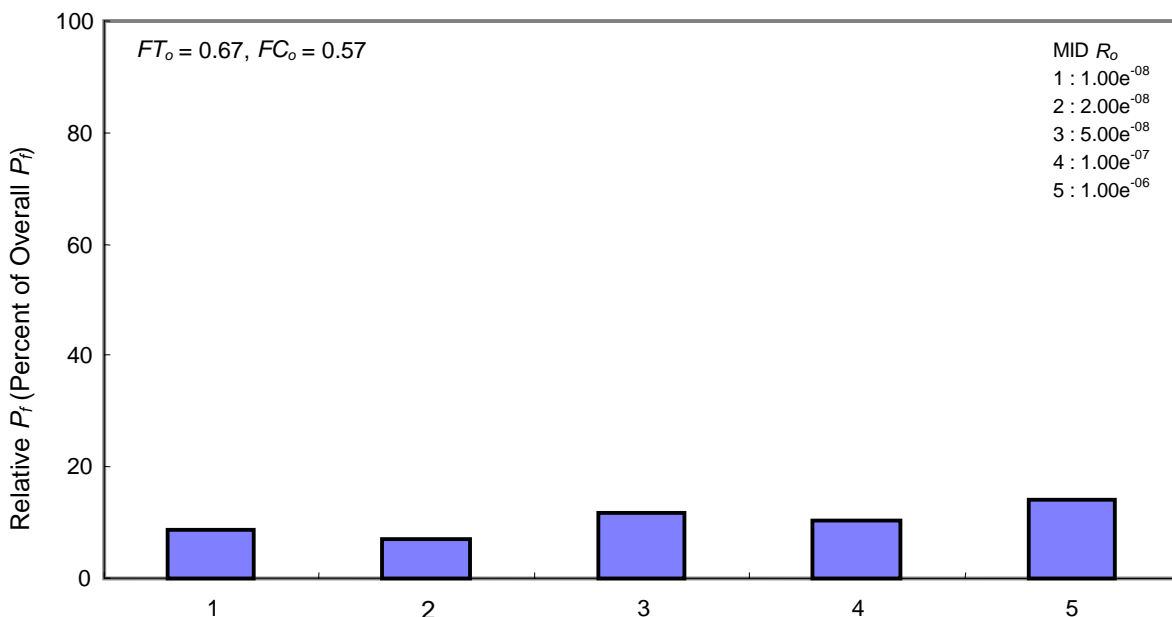


FIGURE 29. RELATIVE P_f FOR LOCATION 28 WITH VARIABLE R_o FOR MID

The relative failure probability is more significantly affected by varying the strength reduction factors. For the three locations discussed above, with values of FC_o at 0.3, 0.5, and 0.7, the results are shown in figures 30 to 32. These figures show that the relative P_f decreases as FC_o increases for the compression skin (Locations 1 and 4, figures 30 and 31), whereas the relative P_f increases with increasing value of FC_o for the tension skin (Location 28, figure 32).

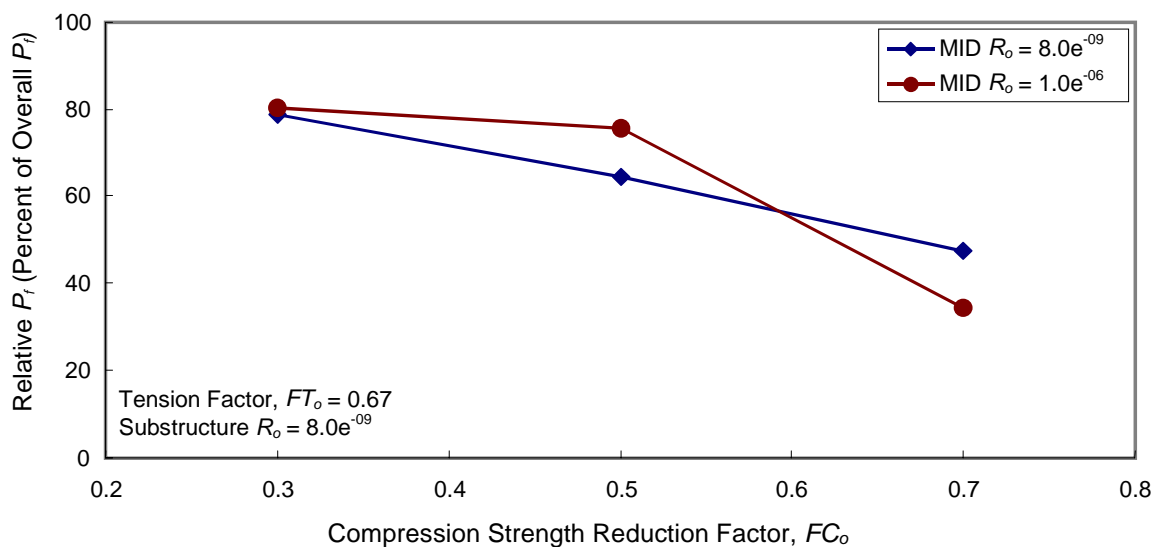


FIGURE 30. RELATIVE P_f FOR LOCATION 1 WITH VARIABLE FC_o FOR MID

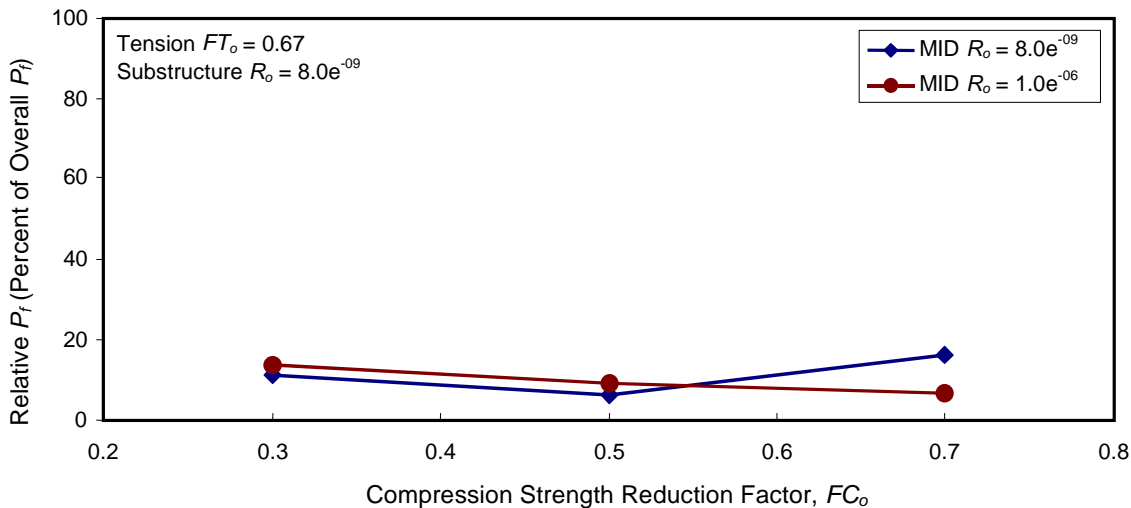


FIGURE 31. RELATIVE P_f FOR LOCATION 4 WITH VARIABLE FC_o FOR MID

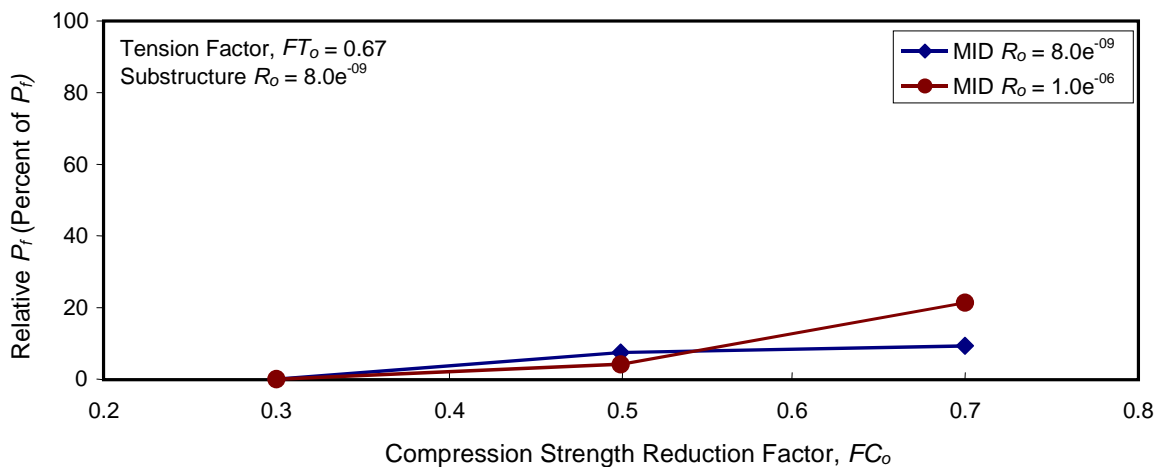


FIGURE 32. RELATIVE P_f FOR LOCATION 28 WITH VARIABLE FC_o FOR MID

In summary, the failure probability is significantly affected by the compression strength reduction factor, FC_o . The damage rate, R_o , only becomes important for small FC_o . Therefore, if impact damage is the most critical damage for damage tolerance consideration, the compression strength after impact (CSAI) will dominate the structural failure probability. Determining CSAI and its distribution is then an important part in the material characterization for probabilistic certification.

3.4 SENSITIVITY OF MANUFACTURING DEFECT PARAMETERS.

The approach for manufacturing defects in the MONTE code is similar to that for operational damage. The three parameters used to characterize the manufacturing defects are, again, damage

rate (R_m), tensile strength reduction factor (FT_m), and compressive strength reduction factor (FC_m). The subscript m refers to manufacturing damage. A sensitivity study was conducted to evaluate the effects of manufacturing defect parameters on the failure probability similar to that conducted for operational damage. The types of defects considered in MONTE are holes, laminate defects such as voids and delaminations, impact, waviness, and tolerance. A single strength is adjusted, as in the case of operational damage, according to the expected frequency, average effect on strength, and location on the aircraft. The defect rate is defined as the expected number of defects per square foot of material.

The values of the parameters used in the sensitivity study are (1) impact rate from 0.00005 to 0.005, (2) tensile strength reduction factor from 0.67 to 0.80, and (3) compression strength reduction factor from 0.3 to 0.7. The results of this study are summarized in table 12. Since the approach for manufacturing defects is similar to that for operational defects, reduced numbers of simulations were performed, as can be seen in table 12. However, the number of simulations is sufficient to establish the sensitivity trend. Significant results are plotted in figures 33 and 34.

TABLE 12. SUMMARY OF THE MANUFACTURING DEFECT
 PARAMETER SENSITIVITY

No. MCS	R_m	FC_m	FT_m	P_f
20,000	0.005	0.3	0.8	$4.940e^{-06}$
70,000	0.005	0.3	0.7	$5.461e^{-06}$
50,000	0.005	0.5	0.7	$1.125e^{-09}$
50,000	0.005	0.7	0.7	$2.842e^{-10}$
20,000	0.0005	0.3	0.8	$8.312e^{-07}$
20,000	0.0005	0.3	0.7	$6.463e^{-07}$
20,000	0.0005	0.5	0.7	$4.209e^{-10}$
100,000	0.0005	0.7	0.7	$3.380e^{-10}$
20,000	0.00005	0.3	0.8	$2.403e^{-08}$
20,000	0.00005	0.3	0.7	$6.735e^{-08}$
20,000	0.00005	0.5	0.7	$3.912e^{-10}$
100,000	0.00005	0.7	0.7	$4.538e^{-10}$

Figure 33 shows the results for an impact rate of 0.005. At a compression strength reduction factor ranging from 0.3 to 0.7, the failure probability ranges over four orders of magnitude. This trend is similar to that of operational defects. Similar results for $R_m = 0.0005$ and 0.00005 are shown in figures 34 and 35, respectively. Table 12 together with figures 33 through 35 indicate that the defect rate has only a slight effect on the failure probability for FC_m larger than 0.5, although the strength reduction factor significantly affects P_f . For small FC_m (see rows 2, 6 and 10) the effect of R_m is significant.

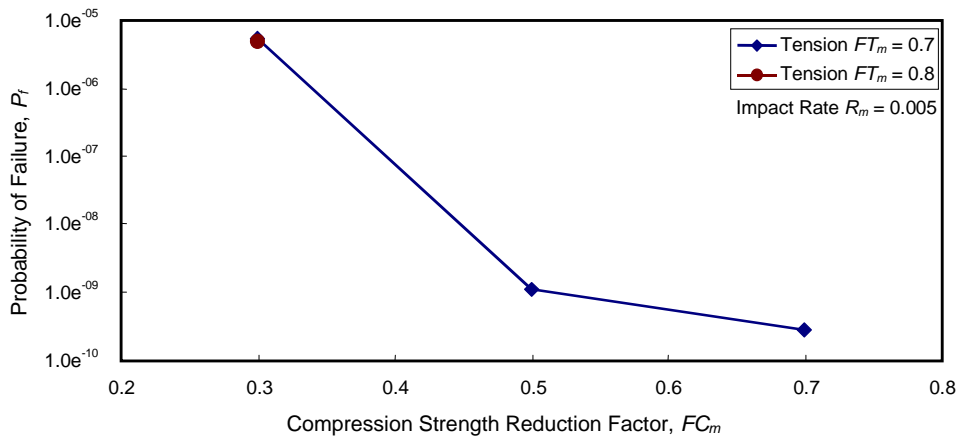


FIGURE 33. INFLUENCE OF THE MANUFACTURING DEFECT PARAMETERS ON P_f , $R_m = 0.005$

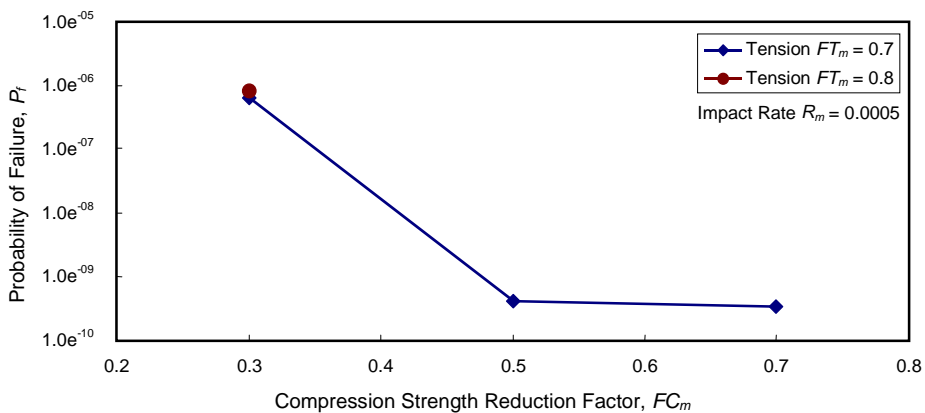


FIGURE 34. INFLUENCE OF THE MANUFACTURING DEFECT PARAMETERS ON P_f , $R_m = 0.0005$

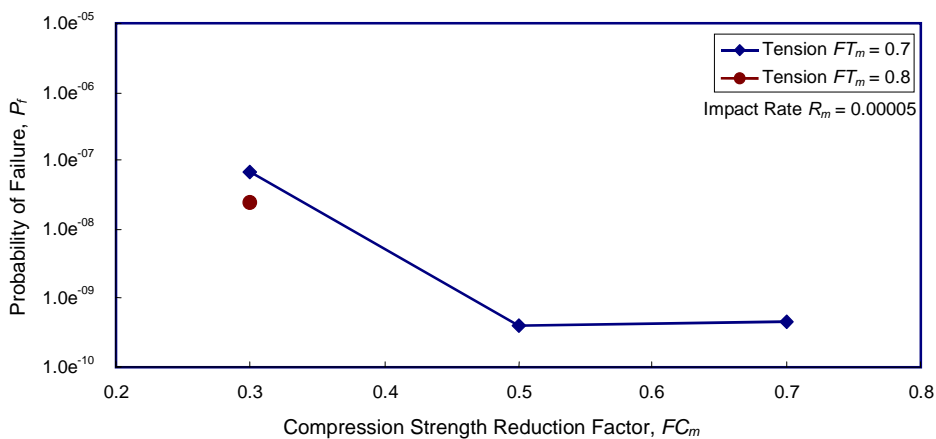


FIGURE 35. INFLUENCE OF THE MANUFACTURING DEFECT PARAMETERS ON P_f , $R_m = 0.00005$

As in the case of operational damage, the parameters for the manufacturing defects also affect the criticality of the structural location. Three critical locations were used to evaluate this effect: one compression critical location (Location 1), one tension critical location (Location 28), and one critical substructure (Location 44). The relative failure probabilities for these locations are shown in figures 36 to 38.

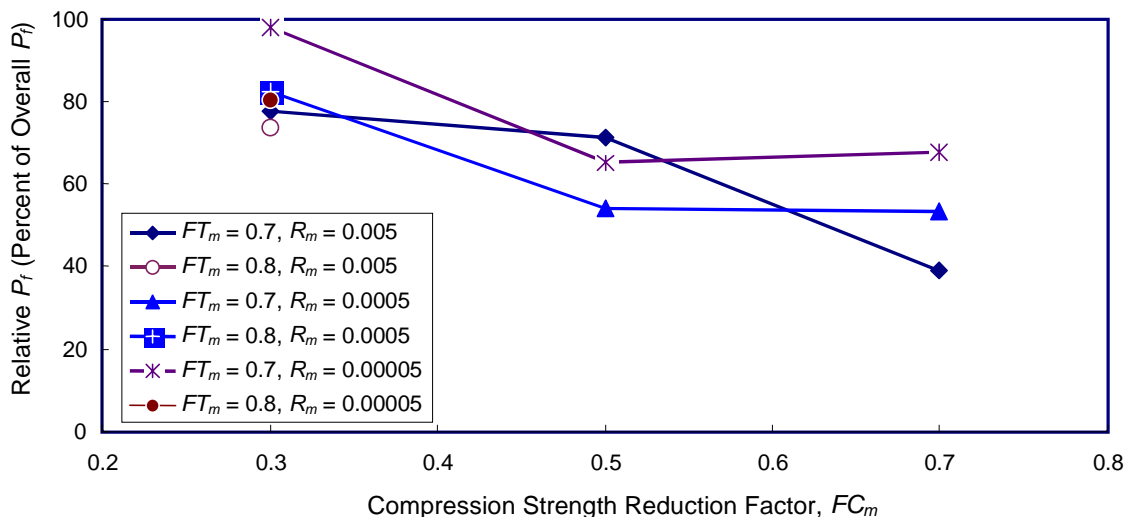


FIGURE 36. RELATIVE P_f SENSITIVITY OF MANUFACTURING DEFECT PARAMETERS AT LOCATION 1 (Critical Compression)

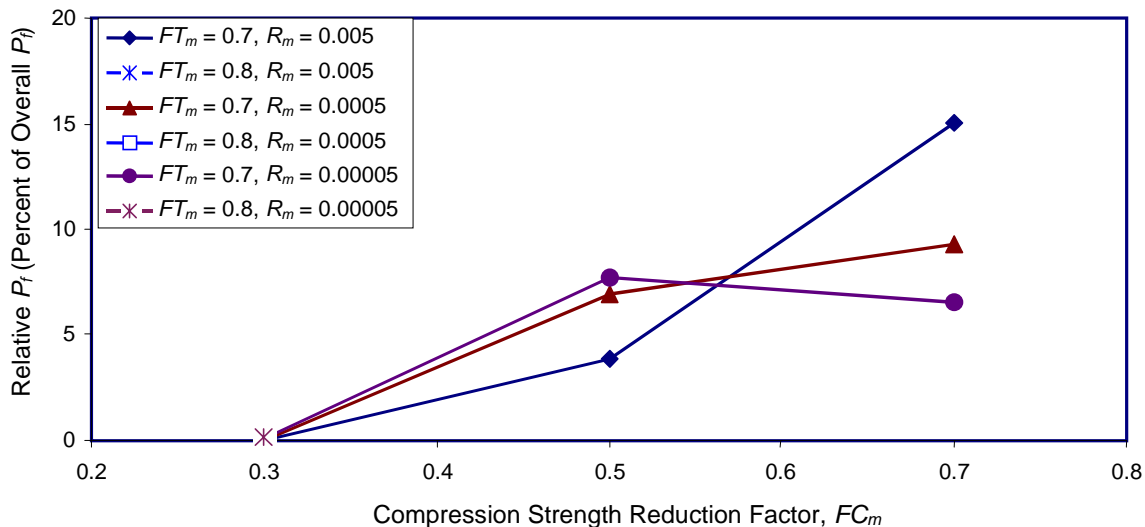


FIGURE 37. RELATIVE P_f SENSITIVITY OF MANUFACTURING DEFECT PARAMETERS AT LOCATION 28 (Critical Tension)

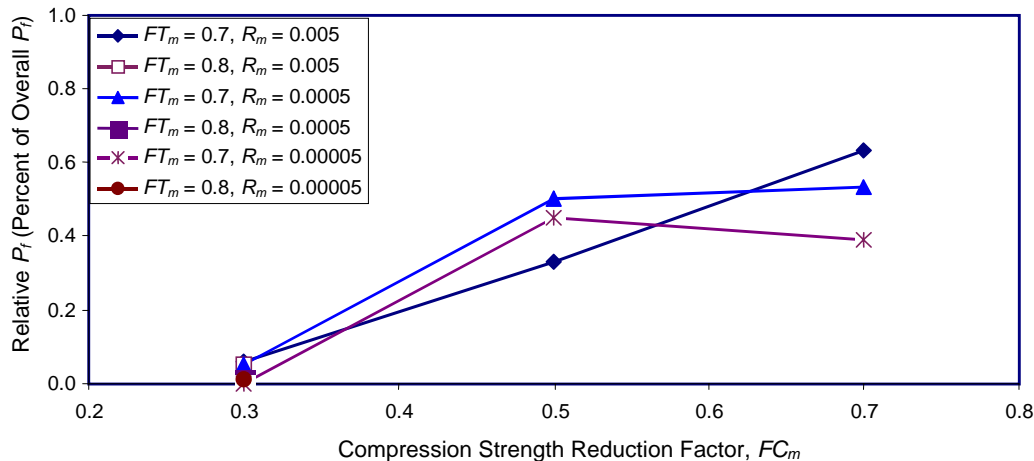


FIGURE 38. RELATIVE P_f SENSITIVITY OF MANUFACTURING DEFECT PARAMETERS AT LOCATION 44 (Critical Substructure)

Figures 36 to 38 show similar trends to those in figures 27 to 32. The overall P_f is dominated by Location 1 on the wing upper surface. The dominance increases as the compressive strength reduction factor (FC_m) decreases.

In summary, the effect of manufacturing defect parameters on the P_f of the structure is similar to that of operational damage. This is because both types of damage have a similar effect on the structural performance. The compressive strength reduction factor has a particularly significant effect on the failure probability. When FC_m increases from 0.3 to 0.7, the value of overall P_f reduces three to four orders of magnitude. The effect of the damage/defect rate, R_m , is of secondary importance at $FC_m = 0.57$ or larger; note that the failure probability remains on the same order of magnitude as R_m changes from 0.005 to 0.00005. However, at $FC_m = 0.3$ the effect of damage rate is significant.

3.5 EQUIVALENT FACTOR OF SAFETY.

Deterministic structural design uses a factor of safety to assure the structural reliability. A factor of safety of 1.5 is generally used for static design of aircraft structures. The level of structural reliability achieved from such a design depends on whether A- or B-basis material allowables were used in design, knowledge of design loads, design assumptions on service environment and inherent/noninspectable damage, and accuracy of analysis methods. For durability and damage tolerance, life factor or load factor is used to account for scatter in a repeated load environment. For both static strength and life, a direct relationship between reliability and deterministic factors of safety or life is difficult to establish.

Both the NGCAD and TsAGI probabilistic methodologies consider damage in the composite structures. For these methods, the relationship between the failure probability and an equivalent factor of safety (EFS) will be established. In the case of the Lear Fan wing structure, the EFS is defined as:

$$EFS = (M.S. + 1) * DS \tag{7}$$

where M.S. is the margin of safety in the static design and DS is the deterministic factor of safety with respect to design limit load. The present sensitivity study will make use of the M.S.'s encountered in the Lear Fan design. The values of DS here range from 1.0 to 1.8. The computed EFS for the critical locations of the Lear Fan wing structure ranges from 1.5 to 5.5. The overall relationship between EFS and P_f is shown in figure 39. This figure shows that there are two or three different relationships between EFS and P_f , each corresponding to a different failure mode and different location. The relationships between the probability of failure and the equivalent factor of safety are similar for the tension and compression. However, for the substructure, the tension members show significantly lower probability of failure comparing to that of the compression members. In addition, the relationship for skin structures and substructures can be separated. In order to examine the different relationships, the results for the compression critical locations are plotted in figure 40 and the results for the tension critical locations are shown in figure 41.

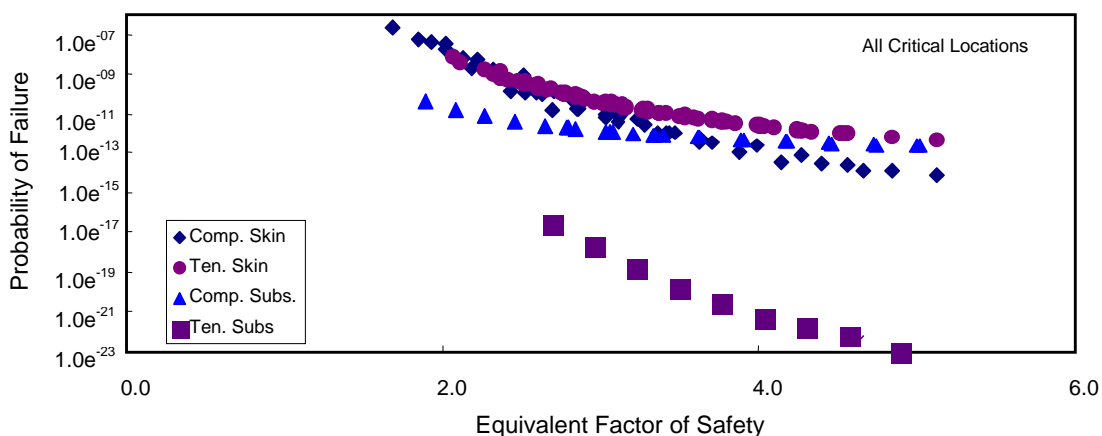


FIGURE 39. PROBABILITY OF FAILURE VERSUS EQUIVALENT FACTOR OF SAFETY

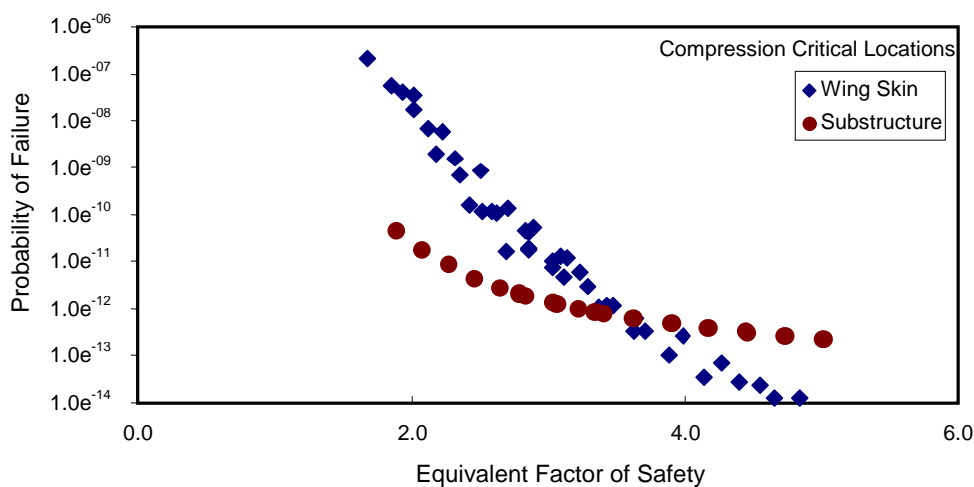


FIGURE 40. PROBABILITY OF FAILURE VERSUS EQUIVALENT FACTOR OF SAFETY FOR THE COMPRESSION CRITICAL LOCATIONS

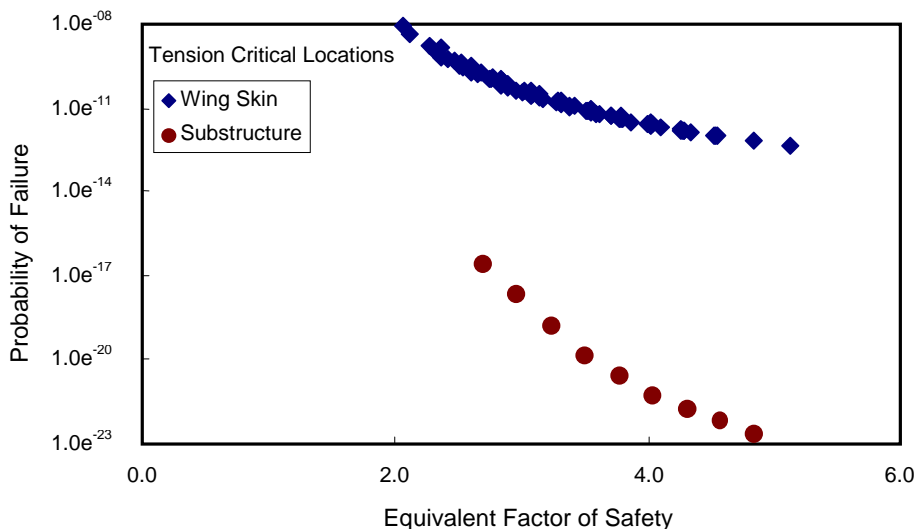


FIGURE 41. PROBABILITY OF FAILURE VERSUS EQUIVALENT FACTOR OF SAFETY FOR THE TENSION CRITICAL LOCATIONS

Both figures 40 and 41 show that there are two distinct functional relationships. In figure 40, the relationship for the skin structure has a steeper slope than that of the substructure. In figure 41, for the tension critical locations, the failure probability is higher for the skin than for the substructure.

In summary, an equivalent factor of safety can be established to determine the relationship between the failure probability and this conventional design parameter. However, for the NGCAD methodology the probability of failure is affected by many factors including damage tolerance parameters, service environment parameters, and load distributions. As a result, a unique relationship between the deterministic design factor and the probability of failure can not be established.

3.6 TRANSPORT WING STRUCTURE.

The second structure for the sensitivity study was a large airplane composite wing used in the USAF/Boeing/NGC “Damage Tolerance of Composites Program” [13]. The wing structure of this transport airplane comprises three primary sections: a constant center section portion and left and right sections that taper in both planform and thickness. The basic wing box is a two-spar configuration with multipanel upper and lower skins that are stiffened by stringers and ribs.

The baseline aircraft for the multirib wing structure design is the Boeing C-X demonstration transport. This transport is a three-engine turbofan aircraft capable of airlifting substantial payload over intercontinental ranges. It is designed to support maximum operational utility and reliability with minimum structural maintenance. The necessary data for the probabilistic analysis are discussed below.

The C-X transport is designed for a service life of 30,000 flight hours with 18,601 landings, including both touch-and-go and small, austere airfield landings. It is assumed that the design

life is 20 years. That would result in an average of 1,500 flight hours per year with an average of 1.613 hours per flight. The 20-year design life was used in reference 13 for moisture content analysis.

The basic skin is a 36-ply (10/80/10) lay-up. The baseline material is AS/3501-6 graphite/epoxy. For the compression skin, the design allowable strain is 6000 μ -in/in. Based on the strain distribution shown in reference 13, the upper wing skin can be divided into five regions. The design strain, the margin of safety, and the surface area for the five regions are given in table 13.

TABLE 13. LOCATIONS FOR THE BOEING C-X WING UPPER SKIN

Location	Strain	Margin of Safety	Area (sq. ft.)
1	5650	0.06	3.46
2	5300	0.13	17.34
3	4590	0.31	7.74
4	3890	0.54	2.92
5	3190	0.88	0.54

The overall temperature distribution was estimated based on the takeoff, landing, and 10 representative mission profiles. The results are shown in table 14.

TABLE 14. OVERALL TEMPERATURE DISTRIBUTION OF THE
C-X TRANSPORT UPPER WING SKIN

Altitude (ft)	Temperature (°F)	Time (Hours)	% Total Lifetime
Takeoff/Landing	180	456.20	1.52
Takeoff/Landing	170	846.50	2.82
Takeoff/Landing	160	189.10	0.63
Takeoff/Landing	150	108.10	0.36
Takeoff/Landing	140	171.10	0.57
0-500	135	1072.20	3.57
500-2,000	132	1933.30	6.44
2,000-4,000	124	6043.47	20.14
4,000-6,000	111	3120.95	10.40
6,000-8,000	98	221.15	0.74
8,000-10,000	85	221.15	0.74
10,000-12,000	72	221.15	0.74
12,000-14,000	59	221.15	0.74
14,000-16,000	46	221.15	0.74
16,000-18,000	34	221.15	0.74
18,000-20,000	21	221.15	0.74
20,000-22,000	8	221.15	0.74
22,000-24,000	-5	221.15	0.74
24,000-26,000	-18	1885.47	6.28
26,000-28,000	-31	435.99	1.45
28,000-30,000	-44	3184.06	10.61
30,000-32,000	-57	3184.06	10.61
>32,000	-67	5379.15	17.93
Total		30,000	100

The computed moisture distribution, based on the analysis conducted in reference 13, is shown in table 15. Table 15 moisture values are expressed in terms of the fraction of the saturated moisture content of 1.4%. The moisture fraction for the 0.3-inch-thick laminate will be used in the analysis.

TABLE 15. ESTIMATED MOISTURE HISTORY FOR THE UPPER WING SKIN
 (values shown represent percentage of the saturated moisture level of 1.4%)

Time (Mo.)	$t = 0.1$ in.	$t = 0.2$ in.	$t = 0.3$ in.	$t = 0.4$ in.	$t = 0.5$ in.
0	0.000	0.000	0.000	0.000	0.000
12	0.539	0.270	0.162	0.135	0.105
24	0.701	0.361	0.248	0.175	0.135
36	0.809	0.464	0.296	0.218	0.167
48	0.879	0.528	0.342	0.261	0.205
60	0.765	0.509	0.350	0.259	0.194
72	0.714	0.512	0.350	0.248	0.197
84	0.695	0.534	0.367	0.270	0.216
96	0.690	0.553	0.394	0.286	0.221
108	0.674	0.580	0.404	0.305	0.237
120	0.655	0.585	0.423	0.313	0.243
132	0.656	0.601	0.445	0.326	0.261
144	0.658	0.598	0.453	0.337	0.270
156	0.801	0.682	0.509	0.377	0.296
168	0.857	0.725	0.547	0.404	0.321
180	0.879	0.755	0.574	0.437	0.342
192	0.914	0.776	0.598	0.461	0.367
204	0.806	0.739	0.601	0.442	0.361
216	0.717	0.709	0.604	0.437	0.356
228	0.701	0.701	0.588	0.458	0.356
240	0.701	0.701	0.593	0.458	0.361

The strength reduction factor for the C-X wing skin material is similar to that of the Lear Fan wing skin. The same environmental strength function was used in the C-X analysis. The C-X structure was designed with the conventional factor of safety of 1.5. However, the load data in reference 13 were not sufficient for a full characterization of the distribution. Based on the load parameter sensitivity, a lognormal load distribution function was assumed with the load distribution parameters $\mu = -0.35$, $\sigma = 0.60$, and $t = 1.0$. The limit load factor is assumed at 3.5 and the cutoff factor is at 150% of limit load.

The manufacturing defect parameters used in the analysis were similar to those used in the Lear Fan analysis. Only the compression skin was analyzed. The values of FC_m for the five defect types are shown in table 16.

TABLE 16. COMPRESSION STRENGTH REDUCTION DUE TO
 MANUFACTURING DEFECTS

Defect Type	FC_m
Hole	0.89
Laminate	0.92
Impact	0.65
Waviness	0.75
Tolerance	0.97

For the operational damage, the occurrence of runway debris impact was assumed to be an unlikely event, and as in the Lear Fan wing study, the damage rate was assumed to be 0 for that type of damage. The damage rate for hail impact was assumed to be identical to that of the Lear Fan upper wing skin. The maintenance induced damage rate was estimated by assuming two 100 ft-lb impacts occurred during the lifetime of the aircraft and each produced an impact area of 10 in² in a five-string panel with area of 800 in². The impact rate is then 8.3e⁻⁰⁷. The compression residual strength for coupons impacted with 100 ft-lb impact energy is approximately 50% of the undamaged laminate. This value, 0.5, was used for FC_o in the analysis, even though it is conservative for full-scale structure.

The failure probability of the wing skin was assessed for the baseline parameters described above. In addition, the sensitivity of the load distribution parameters, the design allowable, and the after-impact compression strength were evaluated.

The effects of the load distribution parameters are presented in table 17. This table presents the effect of varying the design limit load factor (DLLF), distribution mean, standard deviation, and shift factor. The probability of failure for the baseline load distribution (DLLF = 3.5, lognormal mean of -0.35, standard deviation of 0.60, and shift factor of 1.0) is 1.413e⁻⁰⁵, as shown by bold face letters in the table. This value is significantly higher than the baseline failure probability of the Lear Fan wing structure, which ranges from 4.258e⁻¹⁰ to 9.416e⁻¹⁰. This is because the C-X wing design used a higher allowable strain, even though the two structures used comparable material. The allowable strain in the Lear Fan is 5000 μ-in/in, and for the C-X wing it is 6,000 μ-in/in. The after impact compression strength used in the C-X wing analysis was also lower than that used for Lear Fan. The Lear Fan skin used a baseline knockdown factor of 0.57, while on the basis of the impact test data generated in reference 13, the C-X wing used 0.50. In addition, the load distribution parameters used in the C-X wing analysis were estimated from limited available data. The results in table 17 show that the failure probability of the C-X wing is comparable to that of the Lear Fan wing with certain combinations of the load distribution parameters. The table shows that by reducing the standard deviation to values between 0.2 and 0.3 of the load distribution, the C-X wing failure probability is lower than that of the Lear Fan wing.

As just discussed, the compression strength reduction factor (FC_o) in the C-X analysis was lower than that used for the Lear Fan analysis. The sensitivity of P_f to FC_o was evaluated for the C-X structure. The results are listed in table 18. This table shows that the failure probability of the C-X wing is on the same order of magnitude of the Lear Fan wing structure if the value of FC_o is approximately 0.65.

TABLE 17. EFFECTS OF LOAD DISTRIBUTION PARAMETER ON THE
 C-X UPPER WING SKIN P_f

DLLF	Mean	Std. Dev.	Shift Factor	P_f
1.0	-0.35	0.60	1.00	6.720e ⁻⁰³
2.0	-0.35	0.60	1.00	3.273e ⁻⁰⁴
3.0	-0.35	0.60	1.00	3.626e ⁻⁰⁵
3.5	-0.35	0.60	1.00	1.413e⁻⁰⁵
4.0	-0.35	0.60	1.00	5.956e ⁻⁰⁶
5.0	-0.35	0.60	1.00	1.277e ⁻⁰⁶
3.5	-0.10	0.60	1.00	4.368e ⁻⁰⁵
3.5	-0.20	0.60	1.00	2.838e ⁻⁰⁵
3.5	-0.30	0.60	1.00	1.795e ⁻⁰⁵
3.5	-0.35	0.60	1.00	1.413e⁻⁰⁵
3.5	-0.40	0.60	1.00	1.104e ⁻⁰⁵
3.5	-0.50	0.60	1.00	6.614e ⁻⁰⁶
3.5	-0.60	0.60	1.00	3.854e ⁻⁰⁶
3.5	-0.35	0.20	1.00	2.865e ⁻¹⁸
3.5	-0.35	0.30	1.00	1.164e ⁻¹⁰
3.5	-0.35	0.40	1.00	1.115e ⁻⁰⁷
3.5	-0.35	0.50	1.00	2.645e ⁻⁰⁶
3.5	-0.35	0.60	1.00	1.413e⁻⁰⁵
3.5	-0.35	0.70	1.00	3.740e ⁻⁰⁵
3.5	-0.35	0.80	1.00	6.848e ⁻⁰⁵
3.5	-0.35	0.60	0.10	4.111e ⁻⁰⁶
3.5	-0.35	0.60	0.50	6.996e ⁻⁰⁶
3.5	-0.35	0.60	1.00	1.413e⁻⁰⁵
3.5	-0.35	0.60	1.50	2.993e ⁻⁰⁵
3.5	-0.35	0.60	2.00	6.708e ⁻⁰⁵
3.5	-0.35	0.60	2.50	1.606e ⁻⁰⁴

Note: The load distribution PDF is a lognormal function. Values in bold face characters are for the assumed baseline.

TABLE 18. SENSITIVITY OF THE UPPER WING SKIN FAILURE PROBABILITY TO FC_o

FC_o	P_f
0.35	2.328e ⁻⁰³
0.40	6.495e ⁻⁰⁴
0.45	1.310e ⁻⁰⁴
0.50 (baseline)	1.413e⁻⁰⁵
0.55	7.180e ⁻⁰⁷
0.60	1.963e ⁻⁰⁸
0.65	3.598e ⁻¹⁰
0.70	5.654e ⁻¹²

A second parameter that significantly affected the failure probability was the design allowable. A sensitivity study was also conducted on the effect of design allowable strain on the failure probability of the C-X wing. The results of this study are shown in table 19. These results again

show that the C-X wing has similar failure probability as the Lear Fan wing if a comparable design allowable used in the analysis is below 5000 μ -in/in (see figures 5 and 12 for baseline failure probability of the Lear Fan wing).

TABLE 19. SENSITIVITY OF THE WING UPPER SKIN FAILURE PROBABILITY TO DESIGN ALLOWABLE STRAIN

Allowable (μ -in/in)	P_f
3500	$1.122e^{-17}$
4000	$7.746e^{-14}$
4500	$8.996e^{-11}$
5000	$1.963e^{-08}$
5500	$9.687e^{-07}$
6000 (baseline)	$1.413e^{-05}$
6500	$8.370e^{-05}$
7000	$2.752e^{-04}$

It is noted that since the Boeing C-X wing upper skin was designed for a higher strain allowable with a severe damage threat, the probabilistic analyses indicated that the C-X wing has higher probability of failure than the Lear Fan wing. Aside from the issue of uncertainty of the load distribution parameters, the test results for the C-X wing box seemed to agree with the analytical results presented here. That is, the probability of failure of the damaged structure is high ($1.413e^{-05}$) as compared to the commonly expected failure probability of $1.0e^{-09}$ or lower for a transport aircraft structure. The impact damaged wing box test failed at a load corresponding to a strain at the failure region of 4141 μ -in/in. With adjustment of the failure load for a torsional load component, the box failed at approximately 105% of limit load. Based on this failure load, the design ultimate load would be at 6000 μ -in/in. This test result would not provide adequate reliability for the proposed probabilistic certification criteria discussed in the next section.

4. PROBABILISTIC CERTIFICATION METHODOLOGY.

Structural certification is a complicated procedure that involves assuring the strength, durability, damage tolerance, and quality of the structure. Separate requirements and separate efforts are usually needed to certify each of the elements of the structure. Structural certification is usually carried out by a combination of analysis to determine strength, durability and damage tolerance, and test evidence to support the analysis. Certification requirements are well established for the conventional deterministic approaches. However, the equivalent requirements are not currently available for probabilistic approach.

The first requirement that is needed for probabilistic certification is a criterion for the required reliability or the permissible probability of failure. No generally acceptable criterion for the probability of failure of structural components has been established either by the aircraft industry or the government certifying agencies, although for some aircraft systems such as flight controls, a requirement of less than one failure in 10^9 flights is implied in the Federal Aviation Regulations (see AC 25.1309-1A and FAR Part 25.1309) for components whose failure would prevent safe continuation of flight and subsequent landing. A general rule that can be used as a probabilistic

criterion is that no member of a fleet of aircraft should be expected to fail during the design lifetime. In terms of probability of failure per flight hour, the criterion can be expressed as:

$$P_f = 1 / (L * N) \quad (8)$$

where L is the design life of the airplane and N is the number of airplanes in the fleet. In the case of the Lear Fan aircraft, the design lifetime is 15,000 flight hours, and if it is assumed that 500 airplanes are expected in the fleet, then the required probability of failure should be less than $1/(500*15,000) = 1.33e^{-07}$ per flight hour. For commercial transport aircraft, the design lifetime is usually longer and the number of airplanes in a fleet larger than in the case of general aviation aircraft such as the Lear Fan 2100, resulting in a requirement for a much lower probability of failure. For example, if the design lifetime is 30,000 flight hours (as for the C-X airplane) and 2,000 airplanes are expected in a fleet, then the probability of failure should be less than $1/(2000*30000) = 1.67e^{-08}$. Although the computed probability of failure in the sensitivity study of the present program may have seemed to support these probabilistic certification requirements, the failure probability numbers were computed on the basis of admittedly incomplete data and were based on the assumption that the distributions used in the analyses were well characterized. This was not the case because the calculations were made only to illustrate an appropriate approach to probabilistic design and not to carry out an actual analysis. Thus, in order to certify structures, analytical methods must be developed and testing methods must be modified or supplemented to determine the distribution parameters adequately for dependable application of the probabilistic approach to aircraft certification.

4.1 ANALYSIS.

The use of the MONTE code requires data from a separate stress analysis as an input to the MONTE probabilistic assessment, and provides no interaction between the structural mechanics and the probability method. In the current program, significant efforts were devoted to making supplementary calculations to use the MONTE code. To integrate these structural mechanics calculations with the existing MONTE code would require a major addition which is beyond the scope of the present effort. However, analytical needs for improving the current approach have been identified from the structural-certification point of view. They are listed below.

- Lack of adequate load distribution, especially in the upper tail of the load distribution, may be the biggest shortcoming of attempts to apply probabilistic analysis to composite aircraft if a probability of failure of less than 10^{-8} per flight hour is required.
- For composite structures the environmental profile and the material and environment interaction need to be characterized accurately.
- Failure analysis and failure criteria need to be developed for both damaged and undamaged structures. The deterministic approaches usually do not require precise failure analysis because of the application of the factor of safety. As a result, simple failure criteria are sufficient for deterministic design. This is not the case for probabilistic approaches since the accuracy of computed probability of failure depends on the accuracy of the failure prediction.

4.2 TESTING.

Certification testing methodology was discussed in detail in reference 4. A building block approach is still the backbone of certification testing, especially for composites. The certification testing program for the probabilistic approach includes the following:

- Allowable tests should be conducted as in the deterministic approach. However, the required data reduction procedure should be consistent with the probabilistic methods. That is, materials should be characterized by statistical distributions.
- Element tests are needed to verify the failure mode and to verify the statistical distribution.
- Damage tolerance and durability testing of coupons and elements are needed to verify the analytical methods and to establish distributions.
- Subcomponent and component testing are needed to uncover unanticipated hot spots in the structure.
- Probabilistic simulation could be used to replace full-scale testing, provided that the building block testing up to the component level has been successfully conducted and is found to correlate well with analysis.

5. CONCLUSIONS.

The following conclusions may be drawn on the basis of the results of this research project:

1. Because of the difficulty in establishing confidence levels of low probability of failure and data accuracy, the analysis methodologies currently available for probabilistic structural analysis can only be assumed to have an accuracy within an order of magnitude.
2. Supporting data in material properties, load distributions, and other parameters are not sufficient to improve the accuracy. To improve the analytical accuracy and for the purpose of structural certification, statistical distributions that provide the best fit for the data statistics must be generated for these supporting data.
3. The probabilistic certification requirement that no structural failure should occur in the fleet of aircraft during its design lifetime may be successfully achieved, judging from the example problems considered.
4. Current probabilistic certification procedures require improvements in both analysis approach and testing methodology, such as confidence limits and testing replication.
5. If fully developed, probabilistic certification methods can simplify the strength, durability, and damage tolerance certification into a single step procedure.

6. REFERENCES.

1. "Composite Aircraft Structure," Advisory Circular (AC) 20-107A, Federal Aviation Administration, April 25, 1984.
2. Davies, C.R., "Certification of Composites for Commercial Aircraft," Aerospace Technology Conference and Exposition, Anaheim, CA, September 1989, TPS 892212.
3. Soderquist, J.R., "Design/Certification Considerations in Civil Composite Aircraft Structures," Aerospace Technology Conference and Exposition, Long Beach, CA, October 1987, TPS 871846.
4. Whitehead, R.S., Kan, H.P., Cordero, R., and Saether, E.S., "Certification Testing Methodology for Composite Structures," Report No. NADC-87042-60, Volumes I and II, October 1986.
5. Sanger, K.B., "Certification Testing Methodology for Composite Structures," Report No. NADC-86132-60, January 1986.
6. Kan, H.P., Cordero, R., and Whitehead, R.S., "Advanced Certification Methodology for Composite Structures," Final Report, DOT/FAA/AR-96/111, April 1997.
7. Rapoff, A.J., Dill, H.D., and Sanger, K.B., "An Improved Certification Methodology for Composites," Final Report, NADC Contract No. N62269-87-C-0258, August 1989.
8. Kan, H.P., "Delamination Methodology for Composite Structures," Report No. NAWCADWAR-94097-60, DOT/FAA Report No. DOT/FAA/CT-93/64, February 1994.
9. Shah, C.H., Kan, H.P., and Mahler, M., "Certification Methodology for Stiffener Terminations," Report No. DOT/FAA/AR-95/10, April 1996.
10. Gary, P.M. and Riskalla, M.G., "Development of Probabilistic Design Methodology for Composite Structures," Report No. DOT/FAA/AR-95/17, August 1997.
11. Long, M. W. and Narcisco, J., "Probabilistic Design Methodology for Composite Aircraft Structures," Report No. DOT/FAA/AR-99/2, June 1999.
12. Ushakov, A., Kuznetsov, A., Stewart, A., and, Mishulin, I., "Probabilistic Design of Damage Tolerant Composite Aircraft Structures, ProDeCompos," Final Report under Annex 1 to Memorandum of Cooperation AIA/CA-71 between FAA and TsAGI, 1997.
13. Horton, R.E. and Whitehead, R.S., "Damage Tolerance of Composites," Volumes I, II, and III, Report No. AFWAL-TR-87-3030, July 1988.